Available online at www.sciencedirect.com

ScienceDirect

Geochimica et Cosmochimica Acta 139 (2014) 173–189

Geochimica et Cosmochimica Acta

www.elsevier.com/locate/gca

Triple oxygen isotope variations in sedimentary rocks

Naomi E. Levin [a,*], Timothy D. Raub [b], Nicolas Dauphas [c], John M. Eiler [d]

[a] Department of Earth and Planetary Sciences, Johns Hopkins University, 3400 N. Charles Street, 301 Olin Hall, Baltimore, MD 21218, USA
[b] Department of Earth and Environmental Sciences, University of St. Andrews, Irvine Building, KY19 9AL Scotland, UK
[c] Origins Laboratory, Department of Geophysical Sciences, Enrico Fermi Institute, The University of Chicago, 5734 South Ellis Avenue, Chicago, IL 60637, USA
[d] Division of Geological and Planetary Sciences, California Institute of Technology, MC 170-25, 1200 E. California Boulevard, Pasadena, CA 91125, USA

Received 30 November 2012; accepted in revised form 20 April 2014; Available online 9 May 2014

Abstract

Relatively large ($\geqslant 0.2‰$) ^{17}O anomalies in the geologic record have been used to recognize atmospheric processes such as photochemical reactions and to trace changes in the partial pressures of O_2 and CO_2 in Earth's atmosphere through time. However, recent oxygen isotope measurements of terrestrial rocks, minerals and waters also reveal common, smaller (but statistically significant) deviations from a single mass-dependent fractionation line. These subtle anomalies have been explained through differences in mass-dependent isotopic fractionations for various equilibrium and kinetic mechanisms. Here we present triple oxygen isotope data on sedimentary silica and oxides, including Archean and Phanerozoic cherts, and iron formations. The distribution of data reflects the mass fractionation laws of low-temperature precipitation reactions during growth of authigenic minerals, variation in $\Delta^{17}O$ of the waters from which sedimentary minerals precipitate, and equilibrium exchange after initial authigenic formation. We use these results to illustrate the potential for small, mass-dependent variations in $\Delta^{17}O$ values of sedimentary rocks to provide constraints on the environmental and climatic conditions in which they formed.

1. INTRODUCTION

$^{18}O/^{16}O$ ratios of natural materials are widely used as proxies for geologic, biologic and hydrologic processes. ^{17}O is another, less utilized, stable isotope of oxygen whose abundance relative to ^{18}O and ^{16}O is often described as a departure from a reference line with a slope close to 0.5 on a triple oxygen isotope plot (Clayton et al., 1973; Clayton and Mayeda, 1983). Large deviations from this line have been attributed to nucleosynthetic anomalies and mass-independent isotopic fractionations; they have been used in cosmochemistry as tracers of genetic relationships among planetary bodies, in atmospheric chemistry as indirect proxies of marine photosynthetic productivity, and in studies of the history of Earth's atmospheric CO_2 concentrations (Thiemens et al., 1995; Luz et al., 1999; Clayton, 2002; Clayton and Nittler, 2004; Bao et al., 2009). Small deviations from the reference line have been recognized in atmospheric and dissolved O_2 (Matsuhisa et al., 1978; Bender et al., 1994; Luz et al., 1999; Young et al., 2002; Blunier et al., 2002; Hendricks et al., 2005), meteoric waters and atmospheric water vapor (Barkan and Luz, 2005; Luz and Barkan, 2010), and in some silicate minerals (Rumble et al., 2007; Pack and Herwartz, 2014), but they are generally overlooked in analysis of terrestrial rocks and minerals,

* Corresponding author. Tel.: +1 410 516 4317; fax: +1 410 516 4933.
E-mail addresses: nlevin3@jhu.edu (N.E. Levin), timraub@st-andrews.ac.uk (T.D. Raub), dauphas@uchicago.edu (N. Dauphas), eiler@gps.caltech.edu (J.M. Eiler).

http://dx.doi.org/10.1016/j.gca.2014.04.034
0016-7037/

either because they are presumed not to exist or because they are below the level of detection at which most oxygen isotopic measurements are made. However, recent studies that identify mass-dependent triple oxygen isotope variation among earth materials (Rumble et al., 2007; Pack and Herwartz, 2014), combined with studies that show triple oxygen isotopes as faithful recorders of kinetic fractionation and mixing effects within the hydrologic cycle (Landais et al., 2008; Luz and Barkan, 2010; Risi et al., 2010; Uemura et al., 2010; Landais et al., 2012), provide new incentive to explore triple oxygen isotope variation in sedimentary rocks and minerals as an archive of the hydrologic cycle and the silicate weathering budget.

Measurements of $^{17}O/^{16}O$ ratios in sedimentary materials have the potential to expand the utility of traditional oxygen isotope studies, which are typically hampered by the difficulty in discerning the influences of seawater isotopic compositions, temperature of formation, and diagenesis on $\delta^{18}O$ values of authigenic minerals. The goal of this study is to determine whether there are meaningful variations in the triple oxygen isotope compositions of marine authigenic minerals from diverse ages and geological settings and to provide a framework for interpreting such variations.

2. MATERIALS, NOTATION AND METHODS

2.1. Materials

The materials analyzed in this study include Archean and Phanerozoic cherts, Archean rocks from southwest Greenland, and Neoproterozoic and Proterozoic oxides and oxide-bearing silicates from South Africa and Australia (Table 1). These samples are a representative rather than exhaustive suite of materials, and we suggest the findings here should be built upon through future studies that expand this selection (*e.g.*, carbonates, phosphates, organic-bound oxygen).

We also analyzed internationally recognized silicate reference materials, Gore Mountain garnet (UWG-2), NBS-28 silica sand, and San Carlos olivine, which are routinely used to normalize $\delta^{18}O$ values of silicates to the Standard Mean Ocean Water (SMOW) scale (*e.g.*, Clayton and Mayeda, 1983; Valley et al., 1995; Gonfiantini et al., 1995; Eiler et al., 1996) and commonly measured in triple oxygen isotope studies of silicates (Franchi et al., 1999; Miller et al., 1999; Spicuzza et al., 2007; Kusakabe and Matsuhisa, 2008; Ahn et al., 2012; Tanaka and Nakamura, 2013; Pack and Herwartz, 2014). Measurements of additional non-sedimentary materials, such as Amelia albite, San Carlos pyroxene, quartz of various origins, synthetic silica, and a basalt, were included in our dataset for comparison to the results from sedimentary rocks (Table 1).

2.1.1. Archean and Phanerozoic cherts

The Phanerozoic chert samples include dark flint nodules from Stevns Klint, Denmark in the Upper Cretaceous-Danian Chalk Group that formed either from direct precipitation from seawater or replacement of carbonate near the sediment–water interface (Madsen and Stemmerik, 2010). The Phanerozoic cherts also include two Mesozoic radiolarian chert samples from Japan. These represent both the reduced (gray-colored, lower Triassic Kamura Formation) and oxidized (red-colored, lowermost Jurassic Inuyama area chert unit) end-members of allochthonous chert belts that interrupt Mesozoic accretionary terrains for 1000s km along the eastern Japanese margin. These bedded chert successions are considered to represent open-ocean pelagic conditions and both occupied subtropical paleolatitudes at the times of their deposition (Oda and Suzuki, 2000; Ando et al., 2001). The gray chert is part of a decameters-thick layer that is inferred to have been deposited during a global oceanic anoxic event (Isozaki, 1997). The paleomagnetic remanence of red hematite in Triassic–Jurassic boundary radiolarian cherts near Inuyama is consistent with its primary origin. Interformational folds that predate accretion require coloration and cementation of the chert within tens of millions years of its deposition (Oda and Suzuki, 2000; Ando et al., 2001). Cherts in both locations have undergone low-grade regional and contact metamorphism subsequent to accretion (Isozaki et al., 1990; Matsuda and Isozaki, 1991; Isozaki, 1994; Oda and Suzuki, 2000; Ando et al., 2001).

The Archean chert samples are from the Agouron-Griqualand Paleoproterozoic Drilling Project drillcore "GKF", which is supposed to sample the slope toe of a late Archean platform-basin transition (Schröder et al., 2006). The Kamden Member of the Nauga Fm. in the Transvaal Supergroup likely represents early diagenesis of precursor sediments in a slope setting (Fischer and Knoll, 2009). Sampled Kamden cherts range in color from black through gray and yellow to red. These mm-scale, stratiform pigmentation changes presumably reflect shifting redox conditions of Archean bottom- or pore-waters. Because all colors of Kamden chert are brecciated at cm-scales, presumably during compaction, both pigmentation and cementation must have occurred relatively early after deposition.

2.1.2. Southwest Greenland: Archean banded quartz–pyroxene rocks

We sampled a suite of samples from Southwest Greenland that include banded iron formation from the Isua Supracrustal Belt, banded quartz–pyroxene rock from the southwestern end of Akilia Island, and quartz from the Amîtsoq meta-igneous granitoid gneiss at the contact between supracrustal rock and tonalitic gneisses in the southwestern end of Akilia Island. All of the samples have been described in detail in other publications (Table 1). The origin of banded quartz-rich rocks from Akilia Island, Greenland is debated: one argument holds that these rocks are the products of metasomatism of an ultramafic protolith (*e.g.*, Fedo and Whitehouse, 2002; Whitehouse et al., 2009; Lepland and Whitehouse, 2011), whereas the other holds that they are chemical sediments akin to banded iron formations (BIFs) and may hold the earliest evidence for life on Earth (*e.g.*, Mojzsis et al., 1996; Nutman et al., 1997; Manning et al., 2006; Dauphas et al., 2004, 2007). Although there is disagreement about the protoliths of the banded rocks, the oxygen isotope compositions of all of the Archean rocks in southwest Greenland may have

Table 1
Descriptions of materials.

Material ID	Description	Material analyzed	Publication where same or related materials are discussed
High temperature, non-sedimentary materials			
HKD-03-74-19	Hawaiian basalt from 1974 Kilauea flow in Ka'u Desert	Bulk rock	Chemtob et al. (2010)
SC olivine	San Carlos olivine	Olivine	Eiler et al. (1996)
SC pyroxene	San Carlos pyroxene	Pyroxene	–
UWG-2	Gore Mountain garnet	Garnet	Valley et al. (1995)
NBS-28	Silica sand	Quartz	Gonfiantini et al. (1995)
A.Alb	Amelia albite	Albite	Eiler et al. (2000)
Qz1	Quartz, metamorphic transparent vug crystals, Inyo Mountains, CA	Quartz	–
Qz4	Milky quartz crystals, Guanojuato, Mexico	Quartz	–
Qz5	Rose quartz crystals, location unknown	Quartz	–
Qz6	Clear interior of large quartz crystal, location unknown	Quartz	–
GE214	Synthetic silica	Synthetic silica	–
Phanerozoic cherts			
PTKA-18	Gray radiolarian chert, ~251 Ma, Permian–Triassic boundary chert, Kamura Formation, Japan	Chert	Isozaki (1994), Matsuda and Isozaki (1991), Isozaki (1997)
JTJB-63	Red radiolarian chert, 201 Ma, Triassic–Jurassic boundary chert, Inuyama area, Japan	Chert	Oda and Suzuki (2000), Ando et al. (2001)
TDR-SKF-09001	Stevns Klint black flint concretion, ~65 Ma, Denmark, Cretaceous-Tertiary boundary interval	Chert	Madsen and Stemmerik (2010), Christensen et al. (1973)
Archean cherts (Kamden Iron Formation, Transvaal Supergroup, South Africa 2.5 Ga)			
GKF-896.22	Pink chert	Magnetite/hematite chert	Schröder et al. (2006), Heck et al. (2011)
GKF-896.38	Pink chert	Magnetite/hematite chert	Schröder et al. (2006), Heck et al. (2011)
GKF-896.51Y	Yellow chert	Chert, trace magnetite	Schröder et al. (2006), Heck et al. (2011)
GKF-897.10	Black chert	Chert, trace magnetite	Schröder et al. (2006), Heck et al. (2011)
GKF-896.51g	Gray chert	Chert, trace magnetite	Schröder et al. (2006), Heck et al. (2011)
GKF-897.42	Gray chert	Chert, trace magnetite	Schröder et al. (2006), Heck et al. (2011)
Paleoproterozoic and neoproterozoic oxides			
HLBIF	Holowilina ferruginous shale (red), South Australia, ~660–641(?) Ma	Red hematite shale, likely trace clay	Halverson et al. (2007), Halverson et al. (2011)
HLR3	Holowilina ferruginous shale (purple), South Australia, ~660–641(?) Ma	Specularite hematite sand, possibly trace clay, magnetite, and quartz	Preiss (1985), Preiss (2000)
GS-12	Hotazel BIF (almost pure hematite), Hotazel Formation, South Africa, 2.2 Ga, Transvaal Supergroup	Hematite	Tsikos et al. (2003), Raub and Kirschvink (2008)
HMS-2	Hotazel Formation, MnO_2, Mamatwan-type ore, Kalahari, South Africa, 2.2 Ga, Transvaal Supergroup	$Mn_7O_8SiO_4$, Mn_3O_4, trace hematite	Evans et al. (2001), Gutzmer et al. (1995), Kim et al. (2011)
TBP-5B	Hematite, Timeball Hill Formation, South Africa, 2.3 Ga, Transvaal Supergroup	Hematite	Eriksson (1973)
Origin of banded rocks from SW Greenland – descriptions from Dauphas et al. (2004, 2007)			
Banded iron formations from Isua Supracrustal Belt, Isua Island			
IF-G	Well-characterized BIF geostandard from Isua	Powdered whole rock: quartz, magnetite, and minor amphibole, pyrite, apatite and carbonate.	Dauphas et al. (2004, 2007), Govindaraju (1995)
IS-04-06	Well-preserved BIF with fine (mm-scale) quartz–magnetite banding	Quartz, also includes quartz, orthopyroxene, clinopyroxene, amphibole, magnetite, and minor pyrite, pyrrhotite, chalcopyrite, apatite, calcite	Dauphas et al. (2007)

(*continued on next page*)

Table 1 (*continued*)

Material ID	Description	Material analyzed	Publication where same or related materials are discussed
Banded quartz–pyroxene rock from southwestern end of Akilia Island			
92–197	Banded quartz–pyroxene rock, fine-grained portion of rock within the main body that is predominantly a coarsed-grained quartz–pyroxene rock. Same as G91–26.	Primarily quartz	Dauphas et al. (2004)
AK-04-08	Coarse-grained bulk of middle part of the quartz–pyroxene rock	Quartz	Dauphas et al. (2007)
AK-98	Banded quartz–pyroxene	Quartz	Dauphas et al. (2004)
SM/GR/97/5	Banded quartz–pyroxene rock, coarse-grained portion of rock, same locality as 92–197	Quartz	Dauphas et al. (2004), Bolhar et al. (2004)
Meta-igneous rocks at contact between supracrustal rocks and tonalitic gneisses in the southwestern end of Akilia Island			
SM/GR/97/2	Granitoid gneiss with tonalitic to quartz dioritic composition, occurs at southern contact with supracrustal rocks of the Akilia association	Primarily quartz	Dauphas et al. (2004), Kamber and Moorbath, 1998, Whitehouse et al. (1999)
SM/GR97/7	Granitoid gneiss with tonalitic to quartz dioritic composition, occurs at northern contact with the Akilia suite	Primarily quartz	Dauphas et al. (2004), Kamber and Moorbath, 1998, Whitehouse et al. (1999)

been influenced by recrystallization during metamorphic and metasomatic events (Griffin et al., 1980; Dymek and Klein, 1988; Heck et al., 2011).

2.1.3. Proterozoic oxides

The oxide materials examined here are products of various degrees of alteration and recrystallization after authigenic deposition. Paleoproterozoic samples come from the Kalahari Manganese Fields (~2.2 Ga Hotazel Fm.) and the siderite facies of the ~2.3 Ga Timeball Hill Fm.; both are part of the Transvaal Supergroup in South Africa (Eriksson, 1973; Gutzmer and Beukes, 1996). The Hotazel Fm. samples include material from the Mamatwan-type ore deposits (sample HMS-2), which underwent the least hydrothermal alteration in the entire field (Gutzmer and Beukes, 1996; Evans et al., 2001). HMS-2 is composed of a primary authigenic mixture of manganese silicate (braunite), hematite, kutnahorite, and mm-scale Mn-rich calcite concretions (Gutzmer et al., 1995). Early diagenetic (post-compaction ca. 2.2 Ga) manganese oxide (hausmannite, Mn_3O_4) formed partly at the expense of manganese carbonate and was intergrown with a second phase of minor hematite (Evans et al., 2001). Our sample preparation and acid pretreatment (see Section 2.3) will have limited the analyzed material to a mixture of hausmannite and braunite with minor (<5 wt%) hematite. Hausmannite in such abundance is extremely rare in the rock record; other manganese oxides and oxyhydroxides (*e.g.*, MnO, MnO_2 and polymorphs) are metastable in the presence of diagenetic sulfides and chlorites. Manganese oxide from Mamatwan-type ore appears to preserve paramagnetic defect characteristics similar to that produced *in vitro* by bacteria and different from synthetic and hydrothermal manganese oxide precipitates (Kim et al., 2011).

The hematite sample (GS-12) from Hotazel Fm. comes from a drillcore into the very earliest phases of deposition of the iron formation, which onlaps pillow basalts from the ~2.2 Ga Ongeluk Fm. A calcareous glacial dropstone within centimeters of the GS-12 sample in the same drillcore represents one of two documented occurrences of active deglaciation postdating the onset of Ongeluk volcanism (Raub and Kirschvink, 2008), establishing a direct chronostratigraphic and paleogeographic link to underlying "Snowball Earth" deposits of Makganyene Fm. diamictite (Evans et al., 1997). The Timeball Hill Fm. hematite (TBP-5B) reflects thermal decomposition from centimeter-scale siderite nodules that were initially deposited and physically transported in a shallow-water deltaic deposit (Eriksson, 1973). The Timeball Hill Fm. at this "Telegraph Hill" type section was thoroughly calcinated (≫350 °C, French, 1971) to coarsely-crystalline hematite during proximal intrusion of Bushveld complex *ca.* 2060 Ma. Unpublished paleomagnetic results indicate that the hematite crystallized at that age of contact metamorphism. No detectable siderite remains in the rock; and any microcrystalline carbonate phases would have been dissolved by our acid pretreatment.

Holowilina Fm. is a ~660–641 Ma granular iron formation associated with mid-Cryogenian deglaciation in the Adelaide Geosyncline of South Australia. The samples studied here are of two distinct sedimentary facies from the lowest-grade exposures in the basin. Sample HLR3 is a high-energy hematite sandstone preserving centimeter-scale ripple and dune crossbeds. It is likely the shallowest-water Holowilina outcrop exposed in the Geosyncline, sitting closely atop the core of an early Cryogenian-active salt diapir, which would have emerged from the shallow Adelaide Sea as a low island (Preiss, 1985, 2000). HLR3 is in turn closely overlain

(within meters) by another anomalously shallow-water unit: a cross-bedded cap dolostone hosting basal dropstones that mark terminal deglaciation. The hematite grains in HLR3 presumably precipitated from seawater and were sorted and transported in the sedimentary environment of a shallow, cold, tropical archipelago. Sample HLBIF comes from a deeper-water setting though still in the least-metamorphosed (sub-greenschist facies) sector of the basin (Lottermoser and Ashley, 2000) on the flank of Oraparinna diapir. Although this salt anticline was active during late Cryogenian time, Holowilina Fm. is entrained within its margin and so likely was deposited while largely unaffected by diapiric tectonism. Sample HLBIF is an iron shale (Halverson et al., 2007, 2011) hosting glacial dropstones and granule conglomerate trails deposited while sea level remained relatively high long in advance of terminal deglaciation.

Of these four hematite samples analyzed, the Holowilina iron shale sample HLBIF is the least metasomatically and metamorphically altered. Sample HLR3 is exhumed from a somewhat deeper structural level of the Adelaide basin and so has experienced somewhat higher burial metamorphic temperature; however its coarse grain size and relative lack of labile matrix minerals may have limited its expressions of alteration. Hotazel BIF GS-12 is completely undeformed however it appears to belong to a regional terrain that has experienced *ca*. 200–300 °C burial metamorphism and crustal fluid flow between the ages of Bushveld intrusion and subsequent, Geon 19 Kheis orogenesis. Paleomagnetic unblocking spectra indicate that manganese oxide-silicate sample HMS-2 also has experienced this 200–300 °C burial metamorphic event (Evans et al., 2001). Timeball Hill Fm. hematite is the highest-grade (>>350 °C contact metamorphism) sample analyzed.

2.2. Notation

Triple oxygen isotope variation is typically characterized as deviation from an expected relationship between $^{17}O/^{16}O$ and $^{18}O/^{16}O$, defined through a mass law for a mass-dependent isotopic fractionation. This relationship is described by $^{17/16}\alpha_{a-b} = (^{18/16}\alpha_{a-b})^{\theta}$, where $\alpha_{a-b} = R_a/R_b$, R is the ratio of the heavy to light isotope in two materials (a, b), and θ is the triple isotope fractionation exponent which generally varies between 0.500 and 0.5305 for recognized mass-dependent processes of oxygen isotope fractionation (Matsuhisa et al., 1978).

This relationship can be linearized and placed into δ-notation such that $\delta'^{17}O = \theta \times \delta'^{18}O$, where $\delta^x O = ({}^xR_{sample}/{}^xR_{standard} - 1) \times 1000$ and $\delta'^x O = 1000 \times \ln(\delta^x O/1000 + 1)$ (Hulston and Thode, 1965). Deviation from this relationship, $\Delta^{17}O$, is defined as $\Delta^{17}O = \delta'^{17}O - (\lambda_{RL} \times \delta'^{18}O + \gamma_{RL})$, where the slope of the reference line, λ_{RL}, represents an approximation (measured or assigned) of θ and γ_{RL} is the intercept of the reference line and depends on the reference frame used for the isotopic measurements (*e.g.*, sea water or atmospheric O_2) (Miller, 2002; Pack and Herwartz, 2014). The value λ_{RL} can be calculated empirically from a suite of samples known or assumed to have formed following a single mass-dependent fractionation process (*e.g.*, Meijer and Li, 1998; Miller, 2002; Barkan and Luz, 2007; Rumble et al., 2007) or it can be assigned a value that corresponds to θ of a process considered to be an appropriate reference (Wiechert et al., 2004; Pack and Herwartz, 2014).

Although both λ and θ are used to describe the slope of an approximately linear relationship in the triple-isotope diagram, we follow convention in the recent literature by distinguishing between the two for the following reason: θ refers to the mass law governing a specific mass-dependent isotopic fractionation with some known (or knowable) chemical physics basis (*e.g.*, an exchange equilibrium or kinetic isotope effect), whereas λ describes the empirical or assigned relationship among samples and may represent the integrated expression of processes with different θ values (Matsuhisa et al., 1978; Rumble et al., 2007; Cao and Liu, 2011). For example, studies of ^{17}O deviations associated with hydrological processes uniformly use a λ_{RL} of 0.528, which is based on measurements of meteoric waters (*e.g.*, Meijer and Li, 1998; Landais et al., 2006; Barkan and Luz, 2007; Luz and Barkan, 2010) and is close to the θ for liquid–vapor equilibrium fractionation in water, 0.529 (Luz and Barkan, 2010). In contrast, studies of triple oxygen variation in terrestrial minerals and rocks have used empirical measurements of different suites of terrestrial rocks and minerals to define a terrestrial fractionation line ($\lambda = 0.524$–0.527), which is presumed to represent some kind of average of the mass-dependent fractionations by geological materials (*e.g.*, Spicuzza et al., 2007; Kusakabe and Matsuhisa, 2008; Ahn et al., 2012; Hofmann et al., 2012; Tanaka and Nakamura, 2013). Any λ_{RL} value based on analysis of materials with a range of $\delta^{18}O$ values large enough for a statistically robust determination (typically ~ 20‰ or more) likely formed via processes governed by a range of different mass-dependent fractionation relationships (*i.e.*, different θ values; Matsuhisa et al., 1978). Studies of more closely related materials (Rumble et al., 2007) and theoretical models of mass-dependent fractionations (Matsuhisa et al., 1978; Cao and Liu, 2011) indicate that we should expect variation in θ among terrestrial rocks and minerals. For this reason, some studies assign a value for λ_{RL} based on a theoretical quantity, such as 0.5305 (Wiechert et al., 2004; Pack and Herwartz, 2014), which is the high-temperature limit of θ for equilibrium fractionation for triple oxygen isotopes (Matsuhisa et al., 1978). This approach has the advantage that it creates a uniform reference frame that should (at least in principle) have the same meaning in every laboratory. It has the disadvantage that the reference frame it creates is idealized and not verifiable by analysis. In particular, it may mask subtle analytical artifacts that could lead to differences in λ values between labs.

For $\Delta^{17}O$ data to be comparable among different laboratories and studies two criteria must be met: (1) they must be generated from isotopic measurements of $\delta^{18}O$ and $\delta^{17}O$ calibrated to a common reference frame, whether it is a water reference SMOW or a silicate reference such as Gore Mountain garnet, and (2) $\Delta^{17}O$ must be calculated selecting uniform values for λ_{RL} and γ_{RL} (or values that can be accurately related to those adopted by another laboratory).

2.3. Methods

All samples were sieved to recover the 125–250 μm fraction, treated with 0.1 M acetic acid to remove any

carbonate, rinsed with deionized water and dried before analysis. Samples were loaded in the laser-fluorination chamber, evacuated and pretreated with BrF_5 vapor for 12 h prior to laser fluorination to remove adsorbed water and other highly reactive contaminants. Silicate and oxide samples (2–3 mg) were fluorinated with BrF_5 in a laser fluorination extraction system as described by Valley et al. (1995). This system was modified to directly collect and purify O_2 gas using a 13× molecular sieve trap immersed in an ethanol slush (−70 °C), in order to allow O_2 gas to pass through but trap any byproducts of the fluorination reaction that were incondensable on the liquid nitrogen traps at −190 °C upstream on the extraction line (Clayton and Mayeda, 1983). Purified O_2 was collected on a second 13× molecular sieve trap immersed in liquid nitrogen (−190 °C). The collected O_2 was released at 60 °C and expanded into the dual inlet bellows of a Finnigan MAT 252 gas source isotope ratio mass spectrometer, where $^{18}O/^{16}O$ and $^{17}O/^{16}O$ ratios of the O_2 gas were measured alternately with a working reference gas from a commercial tank of ultra high purity O_2 gas.

Multiple measurements of silicate reference materials were made in each analytical session. One "session" typically consisted of 1–2 days of measurements of a set of samples and standards that were introduced to the vacuum chamber together in a single sample holder. Typically 20 specimens, including reference materials, were analyzed in each session. Reference materials included at least 2 measurements of different aliquots of UWG-2 in each analytical session. A summary of the data is reported in Table 2. The raw data and calculations are reported in Table S1. The measurements described in this section were made in the Caltech laboratories for stable isotope geochemistry.

We report both $\delta^{18}O$ and $\delta^{17}O$ values relative to the working O_2 reference gas, referred to as 'tank O_2' (Tables 2 and S1). $\delta^{18}O_{tankO2}$ values are converted to the SMOW scale using measurements of UWG-2 (Gore Mountain garnet) as a secondary standard. We did not measure the tank O_2 reference gas or any of the silicate reference materials directly in reference to O_2 generated from fluorination of SMOW. The average conversion factor for $\delta^{18}O$ between our working O_2 gas reference and the SMOW scale is 1.0282 ± 0.0002 ($n = 31$) for UWG-2, assuming $\delta^{18}O_{SMOW} = 5.8‰$ for UWG-2 (Valley et al., 1995). This approach does not enable conversion of $\delta^{17}O$ and $\Delta^{17}O$ values to the SMOW scale because there are large differences in the reported $\Delta^{17}O$ values for silicate reference materials such as UWG-2, NBS-28 and San Carlos olivine. For example, of the triple oxygen isotope studies that include analyses of Gore Mountain garnet, some report or implicitly assume that its $\Delta^{17}O$ value is similar to SMOW (*e.g.*, Spicuzza et al., 2007; Kusakabe and Matsuhisa, 2008; Rumble et al., 2013), whereas others report that its $\Delta^{17}O$ value is *ca.* 0.1‰ lower than that of SMOW (Tanaka and Nakamura, 2013; Pack and Herwartz, 2014). Given the lack of consensus in $\Delta^{17}O$ values of silicate reference materials relative to SMOW, we report all $\Delta^{17}O$ values in this paper relative to Gore Mountain garnet (GMG), where $\Delta^{17}O_{GMG} = \delta'^{17}O_{tankO2} - (\lambda_{RL} \times \delta'^{18}O_{tankO2} + \gamma_{RL\text{-}GMG})$. We use GMG to define the reference frame because it is measured routinely in triple oxygen isotope studies of silicates, making it possible for the results from our study to be compared to results from previous and future studies that report triple oxygen isotope data for GMG (Franchi et al., 1999; Spicuzza et al., 2007; Kusakabe and Matsuhisa, 2008; Ahn et al., 2012; Tanaka and Nakamura, 2013; Rumble et al., 2013; Pack and Herwartz, 2014).

Once the $\Delta^{17}O$ difference between SMOW and GMG (or some other reference silicate material) is definitively resolved, it should be possible to anchor the $\Delta^{17}O$ values presented here to SMOW such that the data presented here can be compared directly to the triple oxygen isotopic composition of water. This may require a coordinated inter-laboratory study of SMOW, other water reference materials, and several silicate reference materials. For the present, we focus on the variations observed in this study, anchored to the (somewhat arbitrary) GMG reference frame we have selected.

For determinations of $\Delta^{17}O_{GMG}$ for our own measurements, we define λ_{RL} empirically from the regression of $\delta'^{18}O_{tankO2}$ and $\delta'^{17}O_{tankO2}$ values of the high-temperature, non-sedimentary materials that we analyzed. This empirical approach to λ_{RL} is consistent with other triple oxygen isotope studies that use materials from a variety of origins to define λ_{RL} (Miller, 2002; Pack et al., 2007; Spicuzza et al., 2007; Kusakabe and Matsuhisa, 2008; Tanaka and Nakamura, 2013). We have chosen the this approach to defining λ_{RL} because it provides an analytically internally consistent way to evaluate mass fractionation in our data and it serves as a way to compare the triple oxygen isotopic data from sedimentary materials to non-sedimentary materials, even though a different selection of non-sedimentary materials might result in a slightly different λ_{RL}. By reporting raw data from silicate reference materials routinely measured by others, these data can easily be recast if a different approach to defining λ_{RL} is deemed appropriate to examine the data.

Linear regressions of $\delta'^{18}O_{tankO2}$ and $\delta'^{17}O_{tankO2}$ values were determined using both unweighted and error-weighted linear regressions. The unweighted regressions were determined using ordinary least squares regression and the error-weighted regressions were determined with the Isoplot 3.00 program developed by Ludwig (2003), which uses the York (1969) regression algorithm and allows for errors to be assigned to each data point and for the error correlation to be considered in the regression. Considering that many of sample materials were only analyzed 2 or 3 times, a unique error was assigned to each sample material for the purpose of the error-weighted regression, where $\sigma_{assigned} = \sigma_{avg}/\sqrt{n}$, σ_{avg} is the average external standard deviation for samples with 9 or more replicates, and n is the number of replicates for a given sample (Table S2). Errors on the regression results (slopes and intercepts) are reported as 95% confidence intervals.

3. RESULTS

Here we report the triple oxygen isotope results from a selection of materials of non-sedimentary origin and three

Table 2
Summary of triple oxygen isotope results.

Material	Category	N	$\delta^{17}O_{tankO2}$	$\delta^{18}O_{tankO2}$	$\delta'^{17}O_{tankO2}$		$\delta'^{18}O_{tankO2}$		$\delta^{18}O_{SMOW}$	$\Delta^{17}O_{GMG}$	
			Avg	Avg	Avg	1σ	Avg	1σ	Avg	Avg	1σ
GKF-896.22	Archean chert	4	−3.63	−7.41	−3.640	0.33	−7.439	0.60	20.6	−0.120	0.050
GKF-896.38	Archean chert	3	−3.18	−6.57	−3.183	0.10	−6.590	0.20	21.4	−0.112	0.015
GKF-896.51g	Archean chert	4	−2.93	−6.06	−2.932	0.27	−6.080	0.57	22.0	−0.131	0.067
GKF-896.51Y	Archean chert	3	−3.53	−7.19	−3.537	0.33	−7.216	0.61	20.8	−0.135	0.010
GKF-897.10	Archean chert	4	−3.10	−6.37	−3.104	0.48	−6.387	0.84	21.7	−0.140	0.055
GKF-897.42	Archean chert	3	−2.67	−5.53	−2.671	0.01	−5.548	0.03	22.5	−0.151	0.005
JTJB-63	Phanerozoic chert	3	1.80	2.90	1.798	0.06	2.900	0.10	31.2	−0.151	0.017
PTKA-18	Phanerozoic chert	3	1.38	2.10	1.377	0.09	2.098	0.16	30.4	−0.148	0.010
TDR-SKF-09001	Phanerozoic chert	2	3.33	5.75	3.321	0.05	5.738	0.08	34.1	−0.129	0.005
SMGR/97/2	Akilia meta-igneous rock	3	−9.92	−19.49	−9.973	0.24	−19.685	0.45	8.2	0.025	0.058
SMGR97/7	Akilia meta-igneous rock	2	−9.42	−18.50	−9.462	0.04	−18.674	0.001	9.2	0.002	0.036
92–197	Akilia qtz–px rock	3	−8.68	−17.08	−8.723	0.51	−17.226	0.95	10.6	−0.025	0.005
92–197qz	Akilia qtz–px rock	3	−7.35	−14.58	−7.381	0.03	−14.685	0.06	13.2	−0.028	0.021
AK04-08	Akilia qtz–px rock	6	−7.01	−13.93	−7.034	0.14	−14.026	0.28	13.9	−0.029	0.035
AK98	Akilia qtz–px rock	6	−7.75	−15.33	−7.778	0.04	−15.449	0.06	12.4	−0.020	0.036
SMGR/97/5	Akilia qtz–px rock	6	−7.57	−14.98	−7.594	0.10	−15.094	0.15	12.8	−0.024	0.029
IFG	Isua BIF	3	−10.36	−20.17	−10.410	0.03	−20.381	0.03	7.5	−0.043	0.016
IS04–06	Isua BIF	3	−8.46	−16.64	−8.491	0.41	−16.782	0.76	11.1	−0.028	0.005
IS04–06qz	Isua BIF	3	−7.24	−14.35	−7.262	0.07	−14.453	0.07	13.4	−0.031	0.029
HLBIF	Neoproterozoic oxide	3	−8.37	−16.51	−8.402	0.30	−16.648	0.46	11.2	−0.010	0.053
HLR3	Neoproterozoic oxide	2	−7.17	−14.14	−7.199	0.23	−14.242	0.44	13.7	−0.080	0.001
GS-12	Paleoproterozoic oxide	3	−6.48	−12.86	−6.504	0.07	−12.946	0.12	15.0	−0.071	0.008
HMS-2	Paleoproterozoic oxide	3	−14.56	−28.09	−14.665	0.03	−28.490	0.04	−0.7	−0.009	0.009
TBP-5B	Paleoproterozoic oxide	3	−13.86	−26.85	−13.954	0.32	−27.220	0.54	0.6	0.030	0.042
A.Alb	High-temp, non sed	19	−8.51	−16.78	−8.543	0.15	−16.927	0.28	10.9	−0.004	0.065
GE214	High-temp, non sed	9	−8.22	−16.25	−8.255	0.06	−16.379	0.10	11.5	−0.006	0.032
HKD-03-74-19	High-temp, non sed	4	−11.51	−22.40	−11.579	0.04	−22.656	0.07	5.2	−0.009	0.037
NBS-28	High-temp, non sed	17	−9.16	−18.03	−9.200	0.07	−18.193	0.14	9.7	0.009	0.035
Qz1	High-temp, non sed	4	−6.64	−13.24	−6.660	0.14	−13.324	0.25	14.6	−0.027	0.019
Qz4	High-temp, non sed	2	−8.68	−17.14	−8.719	0.11	−17.292	0.20	10.6	0.013	0.000
Qz5	High-temp, non sed	3	−6.45	−12.90	−6.472	0.02	−12.983	0.07	14.9	−0.019	0.016
Qz6	High-temp, non sed	3	−10.03	−19.60	−10.077	0.09	−19.799	0.14	8.0	−0.018	0.014
SC, olivine	High-temp, non sed	9	−11.46	−22.31	−11.526	0.23	−22.564	0.37	5.3	−0.005	0.064
SC, pyroxene	High-temp, non sed	2	−11.35	−22.03	−11.418	0.32	−22.272	0.57	5.6	−0.051	0.020
UWG-2	High-temp, non sed	31	−11.197	−21.829	−11.260	0.12	−22.070	0.20	5.8	0.000	0.052

Average results are reported for N replicate measurements of sample and reference materials. Means of multiple measurements of a single sample material are reported in the columns labeled 'avg'. The columns labeled 1σ list the 1σ error associated with multiple measurements of the material. δ-values are reported in ‰ units relative to the working reference O_2 gas (tank O_2). $\delta^{18}O$ values are converted to the SMOW scale by assuming that the $\delta^{18}O$ value for UWG-2 is 5.8‰, as reported by Valley et al. (1995). $\Delta^{17}O_{GMG}$ values are reported in ‰ units and are calculated from $\delta'^{18}O_{tankO2}$ and $\delta'^{17}O_{tankO2}$ values, where $\lambda_{RL} = 0.529$ and $\gamma_{RL\text{-}GMG} = 0.415$‰. Results are reported to 3 decimal places to avoid rounding errors in calculations of λ and $\Delta^{17}O$. See Table S1 for raw data.

samples suites that include sedimentary and meta-sedimentary rocks (Fig. 1, Fig. 2, Tables 2 and S1). Results of the ordinary least squares and error-weighted regressions are reported in Tables 3 and S2.

3.1. $\delta^{18}O$ results

The materials analyzed span the range of $\delta^{18}O_{SMOW}$ values expected for silicates and oxides, from −0.7‰ to 34.1‰. The $\delta^{18}O_{SMOW}$ values of non-sedimentary materials that include garnet, quartz, albite, olivine, pyroxene and basalt range from 5.2‰ to 14.9‰. Among the sedimentary materials, Archean and Phanerozoic cherts yield $\delta^{18}O_{SMOW}$ values that range from 20.6‰ to 34.1‰ (Fig. 1b). Quartz separates and whole rock samples from Archean quartz–magnetite banded iron formations (BIFs) from Isua, Greenland yield $\delta^{18}O_{SMOW}$ values that range from 7.5‰ to 13.4‰ ($n = 3$) (Fig. 1c). $\delta^{18}O_{SMOW}$ values of Archean banded quartz–pyroxene rocks of debated origin from Akilia, Greenland range from 10.6‰ to 13.9‰ ($n = 5$). Amîtsoq granitoid gneisses on the northern and southern contact of the Akilia suite yield $\delta^{18}O_{SMOW}$ values that range from 8.2‰ to 9.2‰ ($n = 2$). The $\delta^{18}O_{SMOW}$ values Neoproterozoic oxides from Australia range from 11.2‰ to 13.7‰ ($n = 2$) and range between −0.7‰ and 15.0‰ for Paleoproterozoic oxides from South Africa, which include single samples of hematite from the Hotazel BIF of the Timeball Hill Fm. and from the Kalahari manganese field (Fig. 1d).

3.1. Triple oxygen isotope results

Regressions of $\delta'^{18}O_{tankO2}$ and $\delta'^{17}O_{tankO2}$ exhibit a range of λ values (0.522 to 0.531) and γ_{tankO2} values (0.28–0.42) (Fig. 2). The λ and γ values are largely insensitive to the type of regression that was used (error-weighted or unweighted), however the errors on the λ and γ values are sensitive to error assignment in the regression (Tables 3 and S2). The mean square of weighted deviates (MSWD) values on the error-weighted regressions were very low (0.1–0.7) (Table S2), which indicates that the errors assigned to the $\delta'^{18}O_{tankO2}$ and $\delta'^{17}O_{tankO2}$ values are overestimates (Ludwig, 2003). For this reason and for the sake of simplicity, we use the results of the unweighted, least squares regression to explore differences in λ and γ among the samples we analyzed.

The regression results vary with how the results from different materials are grouped (Fig. 2, Table 3). The regression of all samples analyzed in this study results in a line where $\lambda = 0.523 \pm 0.001$ and $\gamma_{tankO2} = 0.28 \pm 0.02$‰. In contrast, regression of data from the definitively non-sedimentary rocks, that represent high-temperature equilibrium processes, including igneous and high-grade meta-igneous garnet, albite, pyroxene, olivine and quartz, yields $\lambda = 0.529 \pm 0.004$ and $\gamma_{tankO2} = 0.41 \pm 0.07$‰. The regression of the data exclusively from the quartz samples results in $\lambda = 0.523 \pm 0.003$ and $\gamma_{tankO2} = 0.31 \pm 0.06$‰, whereas the regression of the data from the cherts alone yields a line where $\lambda = 0.528 \pm 0.002$ and $\gamma_{tankO2} = 0.28 \pm 0.01$‰. The regression of all data excluding the cherts results in a line where $\lambda = 0.526 \pm 0.002$ and $\gamma_{tankO2} = 0.35 \pm 0.04$‰. Data from BIFs and quartz–pyroxene banded rocks from southwestern Greenland form a line with $\lambda = 0.531 \pm 0.002$ and $\gamma_{tankO2} = 0.42 \pm 0.04$‰.

To compare the triple oxygen isotope composition of specific samples to one another, we also calculate $\Delta^{17}O_{GMG}$ values, defining λ_{RL} as the slope of the regression of the non-sedimentary, high-temperature materials (0.529 ± 0.004) and setting γ_{RL} such that the reference line passes through Gore Mountain garnet ($\gamma_{RL\text{-}GMG} = 0.415$‰). There is little variation in $\Delta^{17}O_{GMG}$ values of the samples we analyzed, except for the Archean and Phanerozoic cherts which yield similarly low $\Delta^{17}O_{GMG}$ values (−0.15‰ to −0.11‰) while spanning a 13.5‰ range in $\delta^{18}O_{SMOW}$ values (Fig. 1, Table 2). Of course the distribution of these results is sensitive to the somewhat arbitrary designation of λ_{RL}, but the clustering of the chert data in Fig. 1 reflects the distinct combination of a high λ and a low γ among the cherts that we analyzed (Fig. 2).

4. DISCUSSION

The λ values that we observe for different materials span the range of λ values that have been reported previously for terrestrial materials and is consistent with studies that document variation in mass-dependent oxygen isotope fractionation among terrestrial materials (Matsuhisa et al., 1978; Rumble et al., 2007; Pack and Herwartz, 2014). The λ value that we derive for quartz (0.523 ± 0.003) is within error of the λ value that Rumble et al. (2007) observe for quartz (0.524 ± 0.001). Likewise, the λ for high-temperature materials (0.529 ± 0.004) is consistent with λ values derived for combinations of metamorphic and igneous rocks reported previously, which range from 0.5262 ± 0.0008 and 0.5266 ± 0.0012 for high-temperature high-pressure garnets (Rumble et al., 2007) up to 0.529 ± 0.001 for coesite eclogites (Rumble et al., 2013). The γ_{tankO2} values (0.27–0.41‰) derived from our measurements indicate that all of the materials measured are enriched in $\Delta^{17}O$ relative to the $\Delta^{17}O$ composition of the working reference gas, which originates from ^{17}O-depleted air, as observed in other triple oxygen isotopic studies of silicates that report $\delta^{18}O$ and $\delta^{17}O$ values relative to tank O_2 gas (Miller et al., 1999; Kusakabe and Matsuhisa, 2008).

The largest and most consistent triple oxygen isotope deviation revealed by our data is the distinct regression of the chert data (high λ and low γ) (Fig. 2), which is also apparent in low $\Delta^{17}O_{GMG}$ values (<−0.11‰) (Fig. 1). The distinctions among the regressions derived from different groups of materials, and the chert data in particular, raise the possibility that the triple oxygen isotope composition of silicate and oxide minerals (and perhaps other materials) might provide distinctive constraints on the mechanisms of their formation and/or the sources of fluids from which they precipitated.

We first consider whether the distinctive signature of cherts and other authigenic phases reflects a fundamentally mass-dependent isotopic fractionation having a distinctive mass fractionation law exponent (*i.e.*, slope in a plot of $\delta'^{18}O$ vs. $\delta'^{17}O$), or is instead a subtle expression of

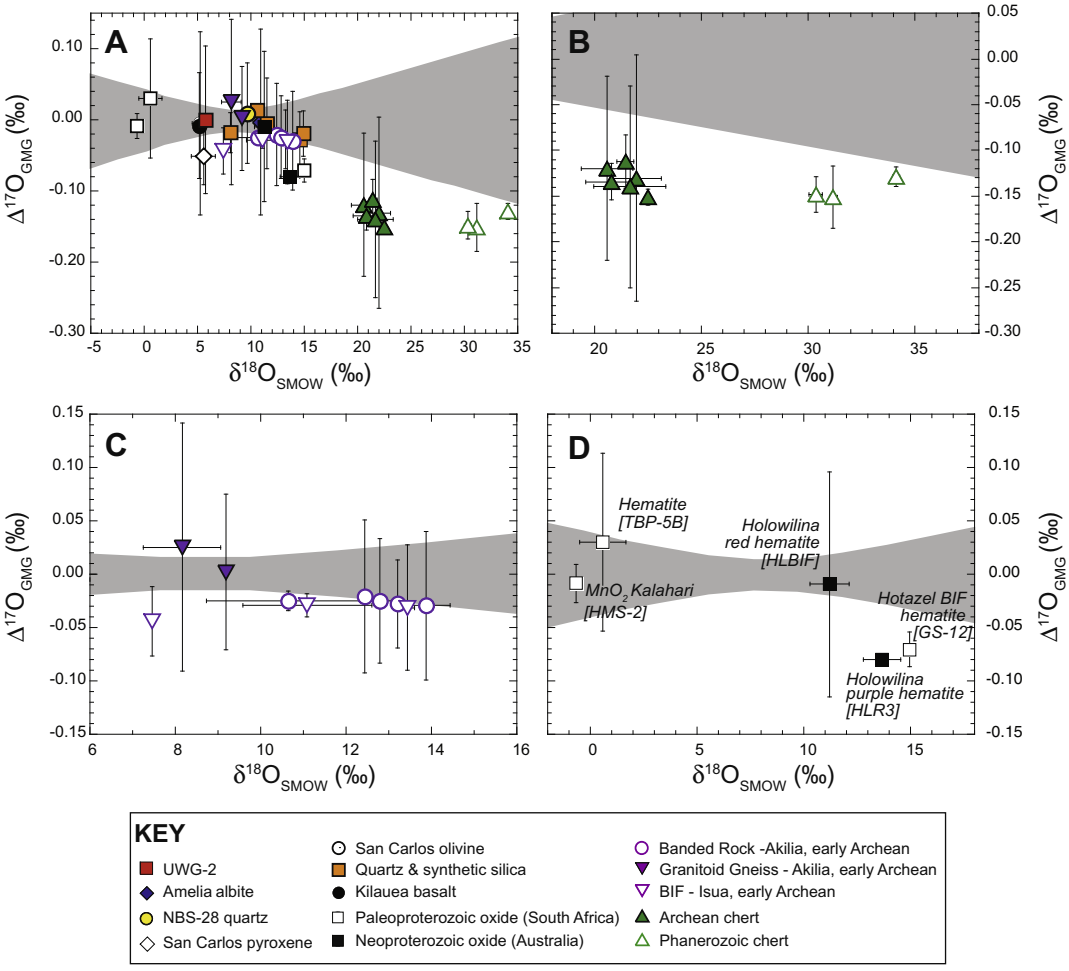

Fig. 1. Triple oxygen isotope results of (A) all materials analyzed in this study and zoomed in views of data from (B) the Archean and Phanerozoic cherts, (C) the Akilia sample suite from southwest Greenland, and (D) Paleoproterozic and Neoproterozoic oxides. Error bars represent the measured 2σ error on replicates; when error bars are missing it is because the error is smaller than the symbol. The gray shading represents the 95% error envelope of the linear regression used to define $\Delta^{17}O$.

mass-independent fractionations (*e.g.*, atmospheric photochemical reactions, as for previous interpretations of the $\Delta^{17}O$ value of atmospheric O_2 and some ancient sulfates). Given the dramatic differences in inferred atmospheric chemistry, particularly pO_2, between the Archean and Phanerozoic, it is tempting to take this as evidence that the triple oxygen isotope composition of cherts reflect some mass-dependent fractionation common to sedimentary silica, rather than as an indirect record of the $\Delta^{17}O$ value of some atmospheric constituent(s). This observation compels us to explore how mass-dependent fractionation could result in non-zero $\Delta^{17}O$ values (or variation in λ and γ values) in sedimentary rocks.

4.1. Scenarios for producing non-zero $\Delta^{17}O$ values by mass-dependent isotopic fractionation

Before discussing specific possible explanations for our observations (Section 4.2), we present several general

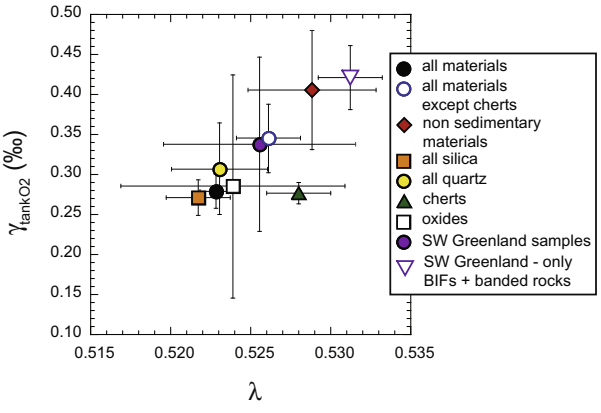

Fig. 2. Scatter plots of the slope (λ) and intercept (γ) derived from least squares linear regressions of $\delta'^{18}O_{tankO2}$ and $\delta'^{17}O_{tankO2}$ values for different groupings of sample materials reported in Table 3. Errors are plotted as the 95% confidence intervals.

Table 3
Results of ordinary least squares regressions of $\delta'^{18}O_{tankO2}$ and $\delta'^{17}O_{tankO2}$ values.

Materials included	Slope (λ)		Y-intercept (γ_{tankO2}) ‰		n[a]	Range in $\delta^{18}O_{SMOW}$‰[b]
	Best Fit	95% conf.	Best Fit	95% conf.		
All materials	0.523	0.001	0.28	0.02	35	−1 to +34
All materials, excluding cherts	0.526	0.002	0.35	0.04	26	−1 to +15
All definitive non-sedimentary materials	0.529	0.004	0.41	0.07	13	+5 to +15
All quartz: NBS28, all Qz samples, GE214, all quartz from SW Greenland	0.523	0.003	0.31	0.06	13	+8 to +15
All silica: NBS-28, all Qz samples, GE214, all chert, Isua BIFs, Akilia quartz–pyroxene banded rocks, quartz Amîtsoq gneiss	0.522	0.002	0.27	0.02	25	+8 to +34
Archean and Phanerozoic Cherts	0.528	0.002	0.28	0.01	9	+21 to +34
All SW Greenland	0.526	0.006	0.34	0.11	10	+8 to +14
SW Greenland: BIFs and quartz–pyroxene banded rocks	0.531	0.002	0.42	0.04	8	+8 to +14
Oxides	0.524	0.007	0.29	0.14	5	−1 to +15

[a] Number of data points used in the regression.
[b] Range in $\delta^{18}O_{SMOW}$ values used the regression, rounded to nearest integer.

scenarios for how variation in $\Delta^{17}O$ (or λ and γ) can be produced from mass-dependent isotopic fractionations during the formation and modification of sedimentary and metasedimentary rocks. Such variation might result from mass-dependent isotopic fractionation in two different contexts: (1) the oxygen isotopic composition of a mineral solely represents authigenic, sedimentary processes (Section 4.1.1), or (2) the oxygen isotopic composition of a mineral represents exchange between solids and fluids or other solids after its initial authigenic formation (Section 4.1.2). These two scenarios differ primarily in the temperatures and water/rock ratios of the environments in which the mineral formation occurs (*i.e.*, relatively cold and water-rich in sedimentary environments vs. hot and water-poor in metamorphic and diagenetic environments).

4.1.1. Non-zero $\Delta^{17}O$ values resulting from sedimentary processes

There are three primary controls on the triple oxygen isotopic composition of an authigenic, sedimentary mineral: the oxygen isotopic composition ($\delta^{18}O$, $\delta^{17}O$) of the water (or fluid) from which the mineral grew, the amplitude of the kinetic or equilibrium isotopic fractionation between water and the mineral ($^{18}\alpha_{mineral-water}$), and the relationship between $^{18}O/^{16}O$ and $^{17}O/^{16}O$ ratios during mineral formation ($\theta_{mineral-water}$). Fig. 3a–c show how variation in these controls will result in predictable differences in the triple oxygen isotopic composition of authigenic sedimentary minerals and how different processes might result in suites of samples with varying $\delta^{18}O$ values but similar $\Delta^{17}O$ values, as we observe for the cherts we analyzed. The scenario depicted in Fig. 3a, where $\Delta^{17}O$ value of waters varies, should be expected in sedimentary systems where kinetic fractionation during evaporation can produce a range in $\Delta^{17}O$ values within water (Landais et al., 2008; Luz and Barkan, 2010). The scenarios where $\theta_{mineral-water}$ varies and where $\theta_{mineral-water} < \lambda_{RL}$, (Fig. 3b and c) should also be expected in sedimentary systems as $\theta_{mineral-water}$ will vary with mineralogy and temperature of formation (Matsuhisa et al., 1978; Rumble et al., 2007; Cao and Liu, 2011).

4.1.2. Modification of $\Delta^{17}O$ values after authigenic formation

Dissolution of a mineral into a pore fluid, re-precipitation of a mineral from this fluid, isotopic exchange between minerals or with waters, and physical mixing of components in a rock can significantly alter the isotopic composition of sedimentary materials after their initial, authigenic formation (*e.g.*, Gregory et al., 1989; Knauth, 1992). In this section we outline ways in which post-depositional, diagenetic, metasomatic and metamorphic processes might alter the triple oxygen isotopic composition of sedimentary and metasedimentary rocks.

For a single event of diagenetic or metamorphic recrystallization in the presence of pore fluid, the $\delta^{18}O$ and $\Delta^{17}O$ values of the resulting modified minerals will reflect: (1) the weighted average isotopic composition of the minerals and fluids participating in the recrystallization reaction, (2) the value of $^{18}\alpha_{mineral-water}$, which will depend on mineral identity, fluid composition and temperature, and (3) θ_{eq} for the mineral-fluid system of interest and temperature of the reaction.

Fig. 3d illustrates a hypothetical situation that is relevant to the oxygen isotope compositions of components of cherts and BIFs, where there is closed-system isotopic exchange between two coexisting mineral phases, quartz and either magnetite, hematite, or a hydrated iron oxyhydroxide precursor. If equilibrium isotopic exchange occurs between magnetite and quartz under diagenetic or metamorphic conditions, as is inferred for many BIFS (*e.g.*, Gregory et al., 1989), the resultant minerals (magnetite – m_e – and quartz – q_e) will plot on a line with a slope, θ_{exc}, indicative of the isotopic fractionation associated with exchange in $\delta'^{17}O$-$\delta'^{18}O$ coordinates that passes through the mean value of the system, M (Fig. 3d). At high temperatures, θ_{exc} associated with equilibrium processes will likely be the same as or close to λ_{RL}, because theoretical estimates for oxygen isotope θ value approach 0.5305 for equilibrium fractionation at temperatures greater than 100 °C (Matsuhisa et al., 1978; Cao and Liu, 2011). If $\theta_{exc} = \lambda_{RL}$, as is depicted in Fig. 3d then the equilibrated products will have a range of $\delta^{18}O$ values that share a similar non-zero $\Delta^{17}O$ value, which is different from

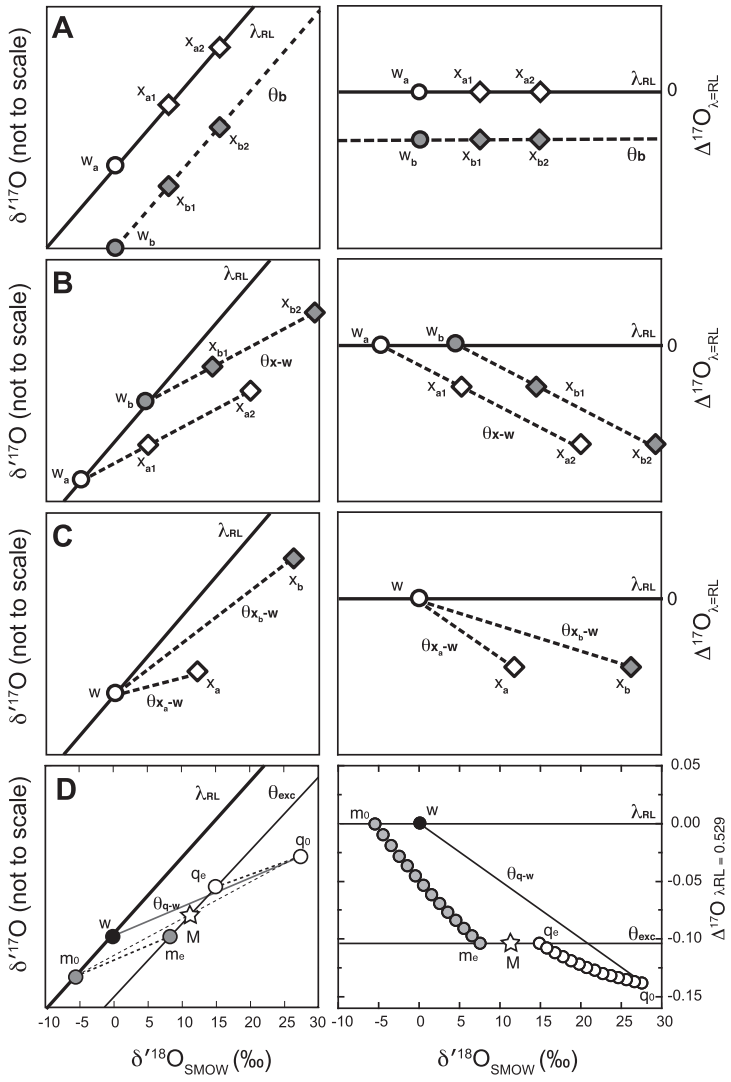

Fig. 3. Scenarios of triple oxygen isotope distributions. For each scenario (A–D), both $\delta'^{18}O$–$\delta'^{17}O$ and $\delta^{18}O$–$\Delta^{17}O$ plots are used because distinctions in $\Delta^{17}O$ are difficult to see on $\delta'^{18}O$–$\delta'^{17}O$ plots. (A) Scenario representing the formation of a mineral from water where w represents the isotopic composition of the water, x represents the isotopic composition of the mineral, and $\alpha_{\text{mineral–water}}$ establishes the difference in δ-values between w and x (subscripts 1 and 2 represents minerals forming at higher and lower temperatures respectively). Subscripts a and b represent the situations where w_a lies on the reference line defined by λ_{RL} and w_b does not. The formation of the minerals x_a and x_b from waters w_a and w_b respectively follow trajectories defined by slopes θ, where $\theta_a = \theta_b = \lambda_{RL}$. (B) The scenario in which a mineral (x) forms from seawater with two different isotopic compositions (w_a, w_b) by a process where $\theta_{x–w}$ defines the slope of the trajectory, $\theta_{x–w} < \lambda_{RL}$, and $\alpha_{\text{x–water}}$ define the position along this trajectory (*e.g.*, x_1, x_2, x). (C) The scenario in which two materials precipitate from seawater with a uniform isotopic composition (w) but follow two different mass-dependent fractionation processes governed by different $\theta_{\text{mineral–water}}$ ($\theta_{xa–w}$, $\theta_{xb–w}$). (D) An example of equilibrium exchange in a closed system between magnetite (m) and quartz (q), where the initial isotopic values (m_0 and q_0) are determined assuming that minerals formed from water with a composition of $\delta^{18}O = 0$, $\delta^{17}O = 0$ at 60 °C, $^{18}\alpha_{\text{mineral–water}}$ for quartz and magnetite follow Clayton et al. (1972) and Zheng, 1991, $\theta_{\text{quartz–water}} = 0.524$ (Rumble et al., 2007), $\theta_{\text{magnetite–water}} = 0.529$, the equilibrium $^{18}\alpha_{\text{magnetite–quartz}}$ at 650 °C follows Chiba et al. (1989) and occurs at $\theta = 0.529$, and the isotopic values after equilibrium isotopic exchange are represented as m_e and q_e. M represents the mean value of the system and lies on the secondary fractionation line, defined by θ_{exc}, which is equivalent to λ_{RL} in this example. This figure is based on the triple oxygen exchange plot shown by Matsuhisa et al. (1978).

the weighted average of the initial $\Delta^{17}O$ values due to the non-linearity of the definition of δ'.

Simple physical mixing of rock components can also result in distinctive $\Delta^{17}O$ signatures because mixing is also not linear in δ' vs. δ' space. This counterintuitive effect arises because mass-dependent fractionations follow an exponential relationship, whereas mixing is linear in the $\delta^{18}O$ vs. $\delta^{17}O$ composition space (Matsuhisa et al., 1978; Farquhar et al., 2007). If a sedimentary rock consists of two or more phases (minerals) that differ from one another in $\delta'^{18}O$, then analysis of a physical mixture of these phases will yield a $\Delta^{17}O$ value different from that of the end members, even when those end members are identical in $\Delta^{17}O$. A corollary of this is that one cannot write a simple mass-balance equation with δ'- and Δ-values as is done with δ values.

4.2. Implications of triple oxygen isotope variation in the rock record

4.2.1. Archean and Phanerozoic Cherts

The origins of cherts and the factors controlling their oxygen isotopic compositions are actively debated (*e.g.*, Knauth and Lowe, 2003; Perry and Lefticariu, 2003; Robert and Chaussidon, 2006; Hren et al., 2009; Marin-Carbonne et al., 2011). In general, chert formation is considered to occur (1) by direct silica precipitation from seawater or hydrothermal waters (biogenically or abiotically) or (2) as a replacement product of precursor materials. In either case, the initial silica may experience dewatering of primary opaline precipitates during diagenesis, metamorphism, or metasomatism (Knauth, 1992; Knauth and Lowe, 2003). The $\delta^{18}O$ values of cherts may reflect temperature-dependent fractionations with respect to seawater, pore waters near the sediment–water interface, or deeper pore or formation waters (Gregory et al., 1989; Knauth, 1992; Knauth and Lowe, 2003; Perry and Lefticariu, 2003; Hren et al., 2009).

The $\delta^{18}O_{SMOW}$ values of the cherts that we analyzed are in agreement with previous studies on the same or similar materials. Previously published $\delta^{18}O_{SMOW}$ values of dark flint nodules from Stevns Klint average 33‰ (Madsen and Stemmerik, 2010) and are similar to the $\delta^{18}O_{SMOW}$ value (34.1‰) reported here. These $\delta^{18}O_{SMOW}$ values indicate water temperatures of approximately 20 °C assuming seawater $\delta^{18}O_{SMOW}$ value of 0‰ and a $\alpha_{chert-water}$ defined by Knauth and Epstein (1976), which is consistent with their formation within centimeters to meters of the sediment-water interface in a shallow sea environment (Madsen and Stemmerik, 2010). The $\delta^{18}O_{SMOW}$ values (30.8 ± 0.6‰) of the two radiolarian chert samples indicate crystallization temperatures of 30 °C, assuming the water $\delta^{18}O_{SMOW} = 0$‰ and $\alpha_{chert-water}$ defined by Knauth and Epstein (1976). We are not aware of any previously published $\delta^{18}O_{SMOW}$ values from these chert belts available for comparison, but these data are consistent with $\delta^{18}O_{SMOW}$ values of late Opal-CT chert and quartz cherts from the bedded radiolarian cherts in the Miocene Monterey Fm. (Behl and Garrison, 1994), bedded cherts from Devonian-Mississippian Arkansas Novaculite (Jones and Knauth, 1979), and other Mesozoic deep-sea cherts (Kolodny and Epstein, 1976).

$\delta^{18}O_{SMOW}$ values for Archean cherts from the Kamden of the Nauga Fm. in the Transvaal Supergroup overlap with $\delta^{18}O_{SMOW}$ values for chert from the Archean Transvaal Iron Fm. (Heck et al., 2011) and plot near the positive end of the range of values observed for Archean cherts that have been used to suggest Proterozoic seawater temperatures of 55–85 °C (*e.g.*, Onverwacht cherts discussed by Knauth and Lowe, 2003). The $\delta^{18}O_{SMOW}$ values of the Kamden cherts are consistent with expectations for chert equilibrated with marine pore fluids during early diagenesis near the sediment surface (Fischer and Knoll, 2009).

The triple oxygen isotope compositions of the Archean and Phanerozoic cherts are distinct from the other materials we analyzed. This distinction can be viewed in terms of both the regression results (Fig. 2) and the low $\Delta^{17}O_{GMG}$ values of the cherts (Fig. 1). If the large range in $\delta^{18}O_{SMOW}$ values of the Archean and Phanerozoic chert samples (20.6–34.1‰) were due solely to differences in temperature of formation ($\alpha_{chert-water}$) and they formed from seawater with a uniform isotopic composition, then we should expect all of the cherts to plot on a line in $\delta'^{18}O$-$\delta'^{17}O$ composition space with a slope that is equivalent to $\theta_{chert-water}$ (Fig. 3a). However, the λ for the cherts (0.528 ± 0.002) is higher than λ for quartz that we measured (0.523 ± 0.003), the λ for quartz measured by Rumble et al. (2007) (0.524 ± 0.001), and the predicted θ for precipitation of quartz in equilibrium with water at low temperatures ($\theta_{qtz-water} = 0.5242$–$0.5255$ for 0–100 °C) (Cao and Liu, 2011). This means either that (1) $\theta_{chert-water} > \theta_{quartz-water}$ (theoretical) or λ_{quartz} (measured), (2) the $\theta_{chert-water}$ for Archean and Phanerozoic cherts is closer 0.524 but they did not form from seawater with uniform $\delta^{18}O$ values, (3) $\theta_{chert-water}$ was lower in the Archean than in the Phanerozoic, or (4) the isotopic composition of the Archean cherts has been modified since authigenic deposition. Given the current data, all of these scenarios are plausible. We briefly review each of them below and present ways they might be tested and used to address the long-standing question of the origin of the relatively low $\delta^{18}O$ values of Archean cherts.

Scenario 1: If the λ value we derive for the cherts is reflective of $\theta_{chert-water}$ and if seawater $\delta^{18}O$ was similar in the Archean and the Phanerozoic, then the $\delta^{18}O_{SMOW}$ values of the Archean cherts would dictate that the Archean cherts formed at temperatures much higher (*ca.* 80 °C) than the Phanerozoic cherts (20–30 °C). This scenario is consistent with studies that explain the large range in chert $\delta^{18}O$ values between the Archean and the Phanerozoic by differences in ocean temperatures (warmer Archean waters) (*e.g.*, Muehlenbachs and Clayton, 1976; Knauth and Epstein, 1976; Holmden and Muehlenbachs, 1993; Knauth and Lowe, 2003). It could be tested by analyzing the triple oxygen isotopic composition of additional chert samples from the Phanerozoic when seawater is considered to be relatively invariant; Phanerozoic cherts should yield a λ value within error of 0.528 ± 0.002 if this is the value for $\theta_{chert-water}$.

Scenario 2: If $\theta_{chert-water}$ were closer to λ values measured previously for quartz (0.524) (Rumble et al., 2007) and the predicted $\theta_{quartz-water}$ (0.524–0.525) (Cao and Liu, 2011), then we might explain the chert data with seawater $\delta^{18}O$ values were lower in the Archean than in the Phanerozoic. This scenario is consistent with studies that explain the increase in chert $\delta^{18}O$ values between the Archean and the Phanerozoic with a *ca.* 10‰ increase in seawater $\delta^{18}O$ (Kasting et al., 2006; Jaffrés et al., 2007). If this scenario is valid then additional triple oxygen isotope analyses should show that Archean and Phanerozoic cherts follow distinct parallel trajectories reflecting the different $\delta^{18}O$ values of the seawater from which they formed. A generic version of this scenario is depicted in Fig. 3b.

Scenario 3: It might also be possible to produce the observed data if seawater $\delta^{18}O$ was relatively invariant but $\theta_{chert-water}$ was lower in the Archean than the Phanerozoic (see Fig. 3c where x_a and x_b would represent the Archean and Phanerozoic cherts, respectively). If this were

the case, lower $\theta_{chert-water}$ in the Archean might reflect higher temperatures during equilibrium fractionation or stronger role of kinetic fractionation during silica deposition in the Archean. We have already discussed higher seawater temperatures in the Archean above in Scenario 1 but the greater influence of kinetic fractionation is also plausible. The silica cycle was intimately linked to the marine carbon and iron cycles in the Archean and earliest Proterozoic (Fischer and Knoll, 2009), when dissolved silica appears to have adsorbed, when possible, to the hydrous surfaces of ferric oxides, which in turn tended to adhere to organic matter during sedimentation through the water column. There would have been ample opportunity for enhanced kinetic fractionations for Archean silica as it migrated through a diagenetic window influenced by multiple mineral surface-modulated reactions.

Scenario 4: Alternatively, diagenetic or metasomatic processes may be responsible for lower $\delta^{18}O$ values in the Archean cherts. If silica deposition from seawater were similar for the Archean and Phanerozoic cherts (with respect to the isotopic composition of the starting seawater, $\theta_{chert-water}$, and temperature of formation), we would expect $\delta^{18}O$ values of the Archean cherts to be 10‰ higher. However the observed values could be explained if diagenetic or metasomatic equilibrium exchange of precursor silica with pore-water or hydrothermal fluids caused a decrease in $\delta^{18}O$ values for the Archean cherts without substantial changes in $\Delta^{17}O$ as outlined in Section 4.1.2 and Fig. 3d.

Distinguishing these scenarios should be possible with additional and more precise data from cherts that represent different time intervals spanning the >10‰ variation in seawater $\delta^{18}O$ for the last 2.5 Gyr that is proposed by Jaffrés et al. (2007). If Scenario 4 is valid then we should expect roughly invariant $\Delta^{17}O$ values among Archean and Phanerozoic cherts despite a range in $\delta^{18}O$ values. If there is temporal variation in $\Delta^{17}O$ values of cherts then it will be possible to explore Scenarios 1, 2 and 3 in more depth.

4.2.2. Southwest Greenland: Archean banded quartz–pyroxene rocks

Our measured $\delta^{18}O$ values of the Akilia quartz-rich rocks, Isua BIFs and the Amîtsoq gneiss are consistent with $\delta^{18}O$ values reported previously. The $\delta^{18}O_{SMOW}$ value of the quartz from the Isua BIF (IS04–06qz), 13.4‰, is close to measurements of similar materials (Heck et al., 2011; Rumble et al., 2013) but toward the low end of the range of $\delta^{18}O_{SMOW}$ values of Isua quartz reported by Perry et al. (1978) (13.0–20.4‰). Whole rock values for the Isua BIF standard, IF-G, are similar to the whole rock value for protosedimentary rock (GR0096) reported by Cates and Mojzsis (2006). We are not aware of $\delta^{18}O_{SMOW}$ values of the quartz from the Amîtsoq gneisses for comparison to our results, but previous studies report whole rock $\delta^{18}O_{SMOW}$ values for these gneisses range from 7.2‰ to 9.2‰ (Cates and Mojzsis, 2006; Manning et al., 2006), which are consistent with the values that we report. Manning et al. (2006) also report whole rock $\delta^{18}O_{SMOW}$ values for the banded quartz–pyroxene rocks from Akilia (11.9‰ to 13.2‰) that overlap in the range of $\delta^{18}O$ values that we report for quartz from similar samples (12.4–13.9‰).

$\Delta^{17}O_{GMG}$ values of the banded quartz–pyroxene rocks from Akilia lie within analytical error of BIFs from Isua Greenland and the Amîtsoq gneisses, which have been used to place age constraints on the banded quartz–pyroxene rocks (Fig. 1c). The relatively large error in the $\Delta^{17}O_{GMG}$ values for the Amîtsoq gneisses, likely due to heterogeneity of the mineral separates, precludes us from making a distinction between the gneisses, the BIFs and the banded quartz–pyroxene rocks. The consistency in $\Delta^{17}O_{GMG}$ values of the banded quartz–pyroxene Akilia rocks and the Isua BIFs, for which the precision is much better, may indicate that they share a similar history of metamorphic re-equilibration between silica and magnetite, with protolith compositions that are consistent with younger, marine cherts. The regression of data from banded quartz–pyroxene Akilia rocks and the Isua BIFs yields λ and γ values that are indistinguishable from the regression of the non-sedimentary materials (Fig. 2). The high λ value (0.531 ± 0.002) may reflect the type of re-equilibration scenario that is described in Section 4.1.2 (Fig. 3d), which would be consistent with reports that indicate a sedimentary origin for the quartz–pyroxene rocks (*e.g.*, Dauphas et al., 2004; Dauphas et al., 2007; Papineau et al., 2010). However the triple oxygen isotope data do not singularly point to a low-temperature, sedimentary origin.

4.2.3. Proterozoic oxides

Several studies examine the oxygen isotopic composition of the quartz and oxide components in Proterozoic iron formations (*e.g.*, Becker and Clayton, 1976; Perry et al., 1978; Gregory et al., 1989), however we are aware of only one study by Tsikos et al. (2003) that specifically reports data from any of the geologic units sampled here. Tsikos et al. (2003) use $\delta^{18}O$ values of carbonates, quartz, magnetite and hematite to assess the role of diagenesis and secondary enrichment on the Hotazel iron formation. They conclude that even the least altered iron formations likely underwent some disequilibrium exchange during burial metamorphism. The $\delta^{18}O_{SMOW}$ value that we measure from Hotazel BIF (15.0‰) is at the high end of the range of values that Tsikos et al. (2003) report for quartz–hematite (9.7–11.8‰), quartz–magnetite (12.8–14.6‰) and pure hematite (−2.9‰ to −0.6‰) from the Hotazel iron formation. The wide range in $\delta^{18}O_{SMOW}$ values of oxides is typical of iron formations and reflects isotopic exchange during the oxidation, leaching or enrichment of the sedimentary oxide protolith (Gregory et al., 1989). Subsequent hydrothermal activity would provide further opportunity for water–rock exchange and the formation of secondary minerals that will contribute to the isotopic variation of these oxides.

The negative $\Delta^{17}O_{GMG}$ values of some of these oxides indicate that they formed from processes characterized by shallow slopes ($\lambda_{oxide} < \lambda_{RL}$) or from waters with low $\Delta^{17}O$ at some point in their history, either during authigenic deposition from seawater or metasomatism. Lower $\Delta^{17}O_{GMG}$ values are generally associated with the least metasomatized hematite samples which may reflect the preservation of some sedimentary signature, whether it is due to kinetic fractionation during oxide precipitation or to variation in equilibrium θ as a function of temperature.

Triple oxygen isotope measurements of paired oxide and quartz samples from individual BIF samples, as has been pursued with $\delta^{18}O$ (*e.g.*, Becker and Clayton, 1976; Gregory et al., 1989), could be a way to further evaluate the diagenetic and exchange history of iron formations and to assess the isotopic exchange history of the silica and oxide components. Continued study of the oxygen isotope fractionation in iron and manganese oxides that includes experimental and theoretical determinations of relevant θ values will further the utility of using mass-dependent triple oxygen isotope variation in iron formations.

5. CONCLUSIONS

Our observations of variation in $\Delta^{17}O$ and mass fractionation lines among sedimentary silica and oxides show that mass-dependent oxygen isotope variations are detectable in the sedimentary rock record and confirm that no single fractionation line exists for terrestrial materials. These observations are consistent with similar scales of variation of $\Delta^{17}O$ values observed in the hydrologic cycle (Uemura et al., 2010), variation in λ among garnets and quartz (Rumble et al., 2007) and crustal materials (Pack and Herwartz, 2014), and recent theoretical estimates for θ (Cao and Liu, 2011). The existence of variation in θ for different terrestrial mass-dependent processes means that we should expect variation in the triple oxygen isotope composition of sedimentary rocks.

We demonstrate the potential for using triple oxygen isotope measurements to test hypotheses about the origin of sedimentary and metasedimentary rocks. The fractionation trajectories proposed in Fig. 3 can be used as a template for asking specific questions about the formation of sedimentary and metasedimentary rocks. For example, if ocean temperature is the only variable responsible for the distribution of $\delta^{18}O$ values between the Archean and Phanerozoic cherts, then precise measurements should show that they lie on a single array in $\delta^{18}O$–$\Delta^{17}O$ space that is characteristic of uniform seawater $\delta^{18}O$ and a constant $\theta_{chert-water}$. However, if the oxygen isotopic composition of the Archean cherts were influenced by post-depositional exchange processes or formed from seawater with a different isotopic composition then we would expect them to plot on arrays that are distinct from those associated with the Phanerozoic cherts. Comparisons of triple oxygen isotope data to predicted arrays, based on differing hypotheses for chert formation, should provide an additional way to test long-standing debates on the trends in chert $\delta^{18}O$ values from the Archean through the Phanerozoic. This approach will complement a suite of analyses that is increasingly used to constrain the origin of cherts, including Si isotopes, Ge/Si ratios, and Si and O isotopes of fluid inclusions (*e.g.*, Grenne and Slack, 2003; Robert and Chaussidon, 2006; Heck et al., 2011; Marin-Carbonne et al., 2011).

Mass-dependent oxygen isotope studies are particularly well suited for investigations of low-temperature processes because small variations in θ result in large variations in $\Delta^{17}O$ when isotope fractionation ($^{18}\alpha_{mineral-water}$) is large, such as is the case during low temperature reactions. Silicates and oxides have been among the first materials analyzed for mass-dependent variation in $\Delta^{17}O$ because of the availability of fluorination techniques, however the abundance of carbonates in the geologic record will make them attractive targets for exploring mass-dependent $\Delta^{17}O$ variation in the future (*i.e.*, once precise methods for measuring $\Delta^{17}O$ values of carbonates are demonstrated), particularly because carbonate clumped-isotope thermometry makes it possible to constrain $^{18}\alpha_{mineral-water}$ (Eiler, 2007). Given theoretical predictions for equilibrium $\theta_{calcite-water}$ values that range from 0.5233 to 0.5239 for 0–100 °C (Cao and Liu, 2011) and large fractionations between $\delta^{18}O$ values of water and calcite at low temperatures, we expect that variations in $\Delta^{17}O$ in carbonates can also be used to evaluate the conditions of mineral precipitation and the triple oxygen isotopic composition of the water from which they formed. Additional triple oxygen isotope measurements of a broad range of materials, interlaboratory calibration of reference materials, and empirical investigations of $\theta_{mineral-water}$ for common Earth surface minerals will increase our ability to use triple oxygen isotope distributions to explore the influence of diagenetic, metasomatic, and metamorphic processes on $\delta^{18}O$ values of sedimentary rocks and thereby increase their utility as tools for probing Earth history.

ACKNOWLEDGMENTS

This study was supported by Caltech Geochemistry and Geobiology Postdoctoral Fellowships and by NSF-EAR0739105 (Raub). We thank Melanie Channon, Sally Newman, Mark Garcia and Steve Chemtob for their help in the laboratory and access to sample materials. We thank Ben Passey and James Farquhar for valuable discussions about these data. We are very grateful to the Associate Editor Qing-Zhu Yin, Executive Editor Marc Norman, and the three reviewers for their thoughtful and instructive reviews of this manuscript.

APPENDIX A. SUPPLEMENTARY DATA

Supplementary data associated with this article can be found, in the online version, at http://dx.doi.org/10.1016/j.gca.2014.04.034.

REFERENCES

Ahn I., Lee J. I., Kusakabe M. and Choi B.-G. (2012) Oxygen isotope measurements of terrestrial silicates using a CO2-laser Br F5 fluorination technique and the slope of terrestrial fractionation line. *Geosci. J.* **16**, 7–16.

Ando A., Kodama K. and Kojima S. (2001) Low-latitude and Southern Hemisphere origin of Anisian (Triassic) bedded chert in the Inuyama area, Mino terrane, central Japan. *J. Geophys. Res.* **B106**, 1,973–1,986.

Bao H., Fairchild I. J., Wynn P. M. and Spötl C. (2009) Stretching the envelope of past surface environments: neoproterozoic glacial lakes from Svalbard. *Science* **323**, 119–122.

Barkan E. and Luz B. (2005) High precision measurements of $^{17}O/^{16}O$ and $^{18}O/^{16}O$ ratios in H_2O. *Rapid Commun. Mass Spectrom.* **19**, 3737–3742.

Barkan E. and Luz B. (2007) Diffusivity fractionations of $H_2{}^{16}O/H_2{}^{17}O$ and $H_2{}^{16}O/H_2{}^{18}O$ in air and their implications for isotope hydrology. *Rapid Commun. Mass Spectrom.* **21**, 2999–3005.

Becker R. H. and Clayton R. N. (1976) Oxygen isotope study of a Precambrian banded iron-formation, Hamersley Range, Western Australia. *Geochim. Cosmochim. Acta* **40**, 1153–1165.

Behl, R. J. and Garrison, R. E. (1994) The origin of chert in the Monterey Formation of California (USA). In *Siliceous, phosphatic and glauconitic sediments of the Tertiary and Mesozoic: Proceedings of the 29th International Geological Congress, Part C* (eds. A. Iijima and R. E. Garrison), Utrecht. pp. 101–132.

Bender M., Sowers T. and Labeyrie L. (1994) The Dole Effect and its variations during the last 130,000 years as measured in the Vostok Ice Core. *Global Biogeochem. Cycles* **8**, 363–376.

Blunier T., Barnett B., Bender M. L. and Hendricks M. B. (2002) Biological oxygen productivity during the last 60,000 years from triple oxygen isotope measurements. *Global Biogeochem. Cycles* **16**, 1029.

Bolhar R., Kamber B. S., Moorbath S., Fedo C. M. and Whitehouse M. J. (2004) Characterisation of early Archaean chemical sediments by trace element signatures. *Earth Planet. Sci. Lett.* **222**, 43–60.

Cao X. and Liu Y. (2011) Equilibrium mass-dependent fractionation relationships for triple oxygen isotopes. *Geochim. Cosmochim. Acta* **75**, 7435–7445.

Cates N. L. and Mojzsis S. J. (2006) Chemical and isotopic evidence for widespread Eoarchean metasedimentary enclaves in southern West Greenland. *Geochim. Cosmochim. Acta* **70**, 4229–4257.

Chemtob S. M., Jolliff B. L., Rossman G. R., Eiler J. M. and Arvidson R. E. (2010) Silica coatings in the Ka'u Desert, Hawaii, a Mars analog terrain: a micromorphological, spectral, chemical, and isotopic study. *J. Geophys. Res.* **115**, E04001.

Chiba H., Chacko T., Clayton R. N. and Goldsmith J. R. (1989) Oxygen isotope fractionations involving diopside, forsterite, magnetite, and calcite: application to geothermometry. *Geochim. Cosmochim. Acta* **53**, 2985–2995.

Christensen L., Fregerslev S., Simonsen A. and Thiede J. (1973) Sedimentology and depositional environment of the Lower Danian Fish Clay from Stevns Klint, Denmark. *Bull. Geol. Soc. Denmark* **22**, 193–212.

Clayton R. N. (2002) Self-shielding in the Solar Nebula. *Nature* **415**, 860–861.

Clayton R. N. and Mayeda T. K. (1983) Oxygen isotopes in eucrites, shergottites, nakhlites, and chassignites. *Earth Planet. Sci. Lett.* **62**, 1–6.

Clayton D. D. and Nittler L. R. (2004) Astrophysics with presolar stardust. *Ann. Rev. Astron. Astrophys.* **42**, 39–78.

Clayton R. N., O'Neil J. R. and Mayeda T. K. (1972) Oxygen isotope exchange between quartz and water. *J. Geophys. Res.* **77**, 3057–3067.

Clayton R. N., Grossman L. and Mayeda T. K. (1973) A component of primitive nuclear composition in carbonaceous meteorites. *Science* **182**, 485–488.

Dauphas N., Zuilen M. v., Wadhwa M., Davis A. M., Marty B. and Janney P. E. (2004) Clues from Fe isotope variations on the origin of Early Archean BIFs from Greenland. *Science* **306**, 2077–2080.

Dauphas N., Zuilen M. v., Busigny V., Lepland A., Wadhwa M. and Janney P. E. (2007) Iron isotope, major and trace element characterization of early Archean supracrustal rocks from SW Greenland: Protolith identification and metamorphic overprint. *Geochim. Cosmochim. Acta* **71**, 4745–4770.

Dymek R. F. and Klein C. (1988) Chemistry, petrology and origin of banded iron-formation lithologies from the 3800 Ma Isua supracrustal belt, West Greenland. *Precambrian Res.* **39**, 247–302.

Eiler J. M. (2007) "Clumped-isotope" geochemistry—the study of naturally-occurring, multiply-substituted isotopologues. *Earth Planet. Sci. Lett.* **262**, 309–327.

Eiler J. M., Valley J. W. and Stolper E. M. (1996) Oxygen isotope ratios in olivine from the Hawaii Scientific Drilling Project. *J. Geophys. Res.* **101**, 11,807–11,813.

Eiler J. M., Crawford A., Elliott T., Farley K. A., Valley J. W. and Stolper E. M. (2000) Oxygen isotope geochemistry of oceanic-arc lavas. *J. Petrol.* **41**, 229–256.

Eriksson K. A. (1973) The Timeball Hill Formation – a fossil delta. *J. Sediment. Petrol.* **43**, 1046–1053.

Evans D. A. D., Beukes N. J. and Kirschvink J. L. (1997) Low-latitude glaciation in the Palaeoproterozoic era. *Nature* **386**, 262–266.

Evans D. A. D., Gutzmer J., Beukes N. J. and Kirschvink J. L. (2001) Paleomagnetic constraints on ages of mineralization in the Kalahari Manganese Field, South Africa. *Econ. Geol.* **96**, 621–631.

Farquhar J., Johnston D. T. and Wing B. A. (2007) Implications of conservation of mass effects on mass-dependent isotope fractionations: influence of network structure on sulfur isotope phase space of dissimilatory sulfate reduction. *Geochim. Cosmochim. Acta* **71**, 5862–5875.

Fedo C. M. and Whitehouse M. J. (2002) Metasomatic origin of quartz–pyroxene rock, Akilia, Greenland, and implications for Earth's earliest life. *Science* **296**, 1448–1452.

Fischer W. W. and Knoll A. H. (2009) An iron shuttle for deepwater silica in Late Archean and early Paleoproterozoic iron formation. *Geol. Soc. Am. Bull.* **121**, 222–235.

French B. M. (1971) Stability relations of siderite ($FeCO_3$) in the System Fe–C–O. *Am. J. Sci.* **271**, 37–78.

Franchi I. A., Wright I. P., Sexton A. S. and Pillinger C. T. (1999) The oxygen-isotopic composition of Earth and Mars. *Meteor. Planet. Sci.* **34**, 657–661.

Gonfiantini R., Stichler W. and Rozanski K. (1995) *Standards and intercomparison materials distributed by the International Atomic Energy Agency for stable isotope measurements*. IAEA, Vienna, IAEA-TECDOC-825. pp 13–29.

Govindaraju K. (1995) Update (1984–1995) on two GIT–IWG Geochemical Reference Samples: Albite from Italy, AL–I and Iron Formation Sample from Greenland, IF-G. *Geostand. Newslett.* **19**, 55–96.

Gregory R. T., Criss R. E. and Taylor, Jr, H. P. (1989) Oxygen isotope exchange kinetics of mineral pairs in closed and open systems: applications to problems of hydrothermal alteration of igneous rocks and Precambrian iron formations. *Chem. Geol.* **75**, 1–42.

Grenne T. and Slack J. F. (2003) Paleozoic and Mesozoic silica-rich seawater: evidence from hematitic chert (jasper) deposits. *Geology* **31**, 319–322.

Griffin W. L., McGregor V. R., Nutman A., Taylor P. N. and Bridgwater D. (1980) Early Archaean granulite-facies metamorphism south of Ameralik, West Greenland. *Earth Planet. Sci. Lett.* **50**, 59–74.

Gutzmer J. and Beukes N. J. (1996) Mineral paragenesis of the Kalahari manganese field, South Africa. *Ore Geol. Rev.* **11**, 405–428.

Gutzmer J., Beukes N. J., Kleyenstuber A. S. E. and Burger A. M. (1995) Magnetic hausmannite from hydrothermally altered manganese ore in the Palaeoproterozoic Kalahari manganese deposit, Transvaal Supergroup, South Africa. *Mineral. Mag.* **59**, 703–716.

Halverson, G.P., Poitrasson, F., Hoffman, P. F., Nedelec, A., and Montel, J. -M. (2007) Iron isotope composition of Neoproterozoic syn-glacial iron-formation: implications for sources and cycling of iron in anoxic oceans. In *7th International Symposium on Applied Isotope Geochemistry, Stellenbosch*, pp. 63–64.

Halverson G. P., Poitrassona F., Hoffman P. F., Nedelec A., Montela J.-M. and Kirby J. (2011) Fe isotope and trace element

geochemistry of the Neoproterozoic syn-glacial Rapitan iron formation. *Earth Planet. Sci. Lett.* **309**, 100–112.

Heck P. R., Huberty J. M., Kita N. T., Ushikubo T., Kozdon R. and Valley J. W. (2011) SIMS analyses of silicon and oxygen isotope ratios for quartz from Archean and Paleoproterozoic banded iron formations. *Geochim. Cosmochim. Acta* **75**, 5879–5891.

Hendricks M. B., Bender M. L., Barnett B. A., Strutton P. and Chavez F. P. (2005) Triple oxygen isotope composition of dissolved O_2 in the equatorial Pacific: a tracer of mixing, production, and respiration. *J. Geophys. Res.* **110**, C12021.

Hofmann M. E. G., Horváth B. and Pack A. (2012) Triple oxygen isotope equilibrium fractionation between carbon dioxide and water. *Earth Planet. Sci. Lett.* **319–320**, 159–164.

Holmden C. and Muehlenbachs K. (1993) The $^{18}O/^{16}O$ ratio of 2-billion-year-old seawater inferred from ancient ocean crust. *Science* **259**, 1733–1736.

Hren M. T., Tice M. M. and Chamberlain C. P. (2009) Oxygen and hydrogen isotope evidence for a temperate climate 3.42 billion years ago. *Nature* **462**, 205–208.

Hulston J. R. and Thode H. G. (1965) Variations in the S^{33}, S^34, and S^{36} contents of meteorites and their relation to chemical and nuclear effects. *J. Geophys. Res.* **70**, 3475–3484.

Isozaki, Y. (1994) Superanoxia across the Permo-Triassic Boundary: record in accreted deep-sea pelagic chert in Japan. In *Pangea: Global Environment and Resources* (eds. A. Embroy, B. Beauchamp, and D. Glass). pp. 805–812.

Isozaki Y. (1997) Permo-Triassic boundary superanoxia and stratified superocean: records from lost deep sea. *Science* **276**, 235–238.

Isozaki Y., Maruyama I. S. and Furuoka F. (1990) Accreted oceanic materials in Japan. *Tectonophysics* **181**, 179–205.

Jaffrés J. B. D., Shields G. A. and Wallmann K. (2007) The oxygen isotope evolution of seawater: a critical review of a long-standing controversy and an improved geological water cycle model for the past 3.4 billion years. *Earth Sci. Rev.* **83**, 83–122.

Jones D. L. and Knauth L. P. (1979) Oxygen isotopic and petrographic evidence relevant to the origin of the Arkansas Novaculite. *J. Sediment. Petrol.* **49**, 581–598.

Kamber B. S. and Moorbath S. (1998) Initial Pb of the Amîtsoq gneiss revisited: implication for the timing of early Archaean crustal evolution in West Greenland. *Chem. Geol.* **150**, 19–41.

Kasting J. F., Howard M. T., Wallmann K., Veizer J., Shields G. and Jaffrés J. (2006) Paleoclimates, ocean depth, and the oxygen isotopic composition of seawater. *Earth Planet. Sci. Lett.* **252**, 82–93.

Kim S. S., Bargar J. R., Nealson K. H., Flood B. E., Kirschvink J. L., Raub T. D., Tebo B. M. and Villalobos M. (2011) Searching for biosignatures using Electron Paramagnetic Resonance (EPR) analysis of manganese oxides. *Astrobiology* **11**, 775–786.

Knauth L. P. (1992) Origin and diagenesis of cherts: an isotopic perspective. In *Isotopic Signatures and Sedimentary Rocks* (eds. N. Clauer and S. Chaudhuri). Springer-Verlag, New York, pp. 123–152.

Knauth L. P. and Epstein S. (1976) Hydrogen and oxygen isotope ratios in nodular and bedded cherts. *Geochim. Cosmochim. Acta* **40**, 1095–1108.

Knauth L. P. and Lowe D. R. (2003) High Archean climatic temperature inferred from oxygen isotope geochemistry of cherts in the 3.5 Ga Swaziland Supergroup, South Africa. *Geol. Soc. Am. Bull.* **115**, 566–580.

Kolodny Y. and Epstein S. (1976) Stable isotope geochemistry of deep sea cherts. *Geochim. Cosmochim. Acta* **40**, 1195–1209.

Kusakabe M. and Matsuhisa Y. (2008) Oxygen three-isotope ratios of silicate reference materials determined by direct comparison with VSMOW-oxygen. *Geochem. J.* **42**, 309–317.

Landais A., Barkan E., Yakir D. and Luz B. (2006) The triple isotopic composition of oxygen in leaf water. *Geochim. Cosmochim. Acta* **70**, 4105–4115.

Landais A., Barkan E. and Luz B. (2008) Record of $\delta^{18}O$ and ^{17}O-excess in ice from Vostok Antarctica during the last 150,000 years. *Geophys. Res. Lett.* **35**, L02709.

Landais A., Steen-Larsen H. C., Guillevic M., Masson-Delmotte V., Vinther B. and Winkler R. (2012) Triple isotopic composition of oxygen in surface snow and water vapor at NEEM (Greenland). *Geochim. Cosmochim. Acta* **77**, 304–316.

Lepland A. and Whitehouse M. J. (2011) Metamorphic alteration, mineral paragenesis and geochemical re-equilibration of early Archean quartz–amphibole-pyroxene gneiss from Akilia, Southwest Greenland. *Int J Earth Sci* **100**, 1–22.

Lottermoser B. G. and Ashley P. M. (2000) Geochemistry, petrology and origin of Neoproterozoic ironstones in the eastern part of the Adelaide Geosyncline, South Australia. *Precambrian Res.* **101**, 49–67.

Ludwig K. R. (2003) *ISOPLOT 3.0, A geochronological toolkit for Microsoft Excel*. Berkely Geochronology Center.

Luz B., Barkan E., Bender M. L., Thiemens M. H. and Boering K. A. (1999) Triple-isotope composition of atmospheric oxygen as a tracer of biosphere productivity. *Nature* **400**, 547–550.

Luz B. and Barkan E. (2010) Variations of $^{17}O/^{16}O$ and $^{18}O/^{16}O$ in meteoric waters. *Geochim. Cosmochim. Acta* **74**, 6276–6286.

Madsen H. B. and Stemmerik L. (2010) Diagenesis of flint and porcellanite in the Maastrichtian Chalk at Stevs Klint, Denmark. *J. Sediment. Res.* **80**, 578–588.

Manning C. E., Mojzsis S. J. and Harrison T. M. (2006) Geology, age and origin of supracrustal rocks at Akilia, West Greenland. *Am. J. Sci.* **306**, 303–366.

Marin-Carbonne J., Chaussidon M., Boiron M.-C. and Robert F. (2011) A combined in situ oxygen, silicon isotopic and fluid inclusion study of a chert sample from Onverwacht Group (3.35 Ga, South Africa): new constraints on fluid circulation. *Chem. Geol.* **286**, 59–71.

Matsuda T. and Isozaki Y. (1991) Well-documented travel history of Mesozoic pelagic chert in Japan: from remote ocean to subduction zone. *Tectonics* **10**, 475–499.

Matsuhisa Y., Goldsmith J. R. and Clayton R. N. (1978) Mechanisms of hydrothermal crystallization of quartz at 250 °C and 15 kbar. *Geochim. Cosmochim. Acta* **42**, 173–182.

Meijer H. A. J. and Li W. J. (1998) The use of electrolysis for accurate $\delta^{17}O$ and $\delta^{18}O$ isotope measurements in water. *Isotopes Environ. Health Stud.* **34**, 349–369.

Miller M. F., Franchi I. A., Sexton A. S. and Pillinger C. T. (1999) High precision $\delta^{17}O$ isotope measurements of oxygen from silicates and other oxides: method and applications. *Rapid Commun. Mass Spectrom.* **13**, 1211–1217.

Miller M. F. (2002) Isotopic fractionation and the quantification of ^{17}O anomalies in the oxygen three-isotope system: an appraisal and geochemical significance. *Geochim. Cosmochim. Acta* **66**, 1881–1889.

Mojzsis S. J., Arrhenius G., McKeegan K. D., Harrison T. M., Nutman A. P. and Friend C. R. L. (1996) Evidence for life on Earth before 3,800 million years ago. *Nature* **384**, 55–58.

Muehlenbachs K. and Clayton R. N. (1976) Oxygen isotope composition of the oceanic crust and its bearing on seawater. *J. Geophys. Res.* **81**, 4365–4369.

Nutman A. P., Mojzsis S. J. and Friend C. R. L. (1997) Recognition of $\geqslant$3850 Ma water-lain sediments in West Greenland and their significance for the early Archean Earth. *Geochim. Cosmochim. Acta* **61**, 2475–2484.

Oda H. and Suzuki H. (2000) Paleomagnetism of Triassic and Jurassic red bedded chert of the Inuyama area, central Japan. *J. Geophys. Res.* **B105**, 25743–25767.

Pack A. and Herwartz D. (2014) The triple oxygen isotope composition of the Earth mantle and understanding ^{17}O variations in terrestrial rocks and minerals. *Earth Planet. Sci. Lett.* **390**, 138–145.

Pack A., Toulouse C. and Przybilla R. (2007) Determination of oxygen triple isotope ratios of silicates without cryogenic separation of NF_3 – technique with application to analyses of technical O_2 gas and meteorite classification. *Rapid Commun. Mass Spectrom.* **21**, 3721–3728.

Papineau D., Gregorio B. T. D., Cody G. D., Fries M. D., Mojzsis S. J., Steele A., Stroud R. M. and Fogel M. L. (2010) Ancient graphite in the Eoarchean quartz–pyroxene rocks from Akilia in southern West Greenland I: petrographic and spectroscopic characterization. *Geochim. Cosmochim. Acta* **74**, 5862–5883.

Perry, Jr, E. C. and Lefticariu L. (2003) Formation and geochemistry of Precambrian cherts. In *Treatise on Geochemistry* (eds. H. D. Holland and K. K. Turekian). Pergamon, Oxford, pp. 99–113.

Perry, Jr, E. C., Ahmad S. N. and Swulius (1978) The oxygen isotope composition of 3,800 m.y. old metamorphosed chert and iron formation from Isukasia, West Greenland. *J. Geol.* **86**, 223–239.

Preiss W. V. (1985) Stratigraphy and tectonics of the Worumba Anticline and associated intrusive breccias. *South Aust. Geol. Survey Bull.* **52**, 85.

Preiss W. V. (2000) The Adelaide Geosyncline of South Australia and its significance in Neoproterozoic continental reconstruction. *Precambrian Res.* **100**, 21–63.

Raub T. D. and Kirschvink J. L. (2008) A Pan-Precambrian link Between deglaciation and environmental oxidation. In *Antarctica: A Keystone in a Changing World. Proceedings of the 10th International Symposium on Antarctic Earth Sciences* (eds. A. K. Cooper, P. J. Barrett, B. Stagg, B. Storey, E. Stump, W. Wise and the 10th ISAES Editorial Team). National Academies Press, Washington, DC, USA, pp. 83–90.

Risi C., Landais A., Bony S., Jouzel J., Masson-Delmotte V. and Vimeux F. (2010) Understanding the ^{17}O excess glacial-interglacial variations in Vostok precipitation. *J. Geophys. Res. Atmos.* **115**, D10112.

Robert F. and Chaussidon M. (2006) A palaeotemperature curve for the Precambrian oceans based on silicon isotopes in cherts. *Nature* **443**, 969–972.

Rumble D., Miller M. F., Franchi I. A. and Greenwood R. C. (2007) Oxygen three-isotope fractionation lines in terrestrial silicate minerals: an inter-laboratory comparison of hydrothermal quartz and eclogitic garnet. *Geochim. Cosmochim. Acta* **71**, 3592–3600.

Rumble D., Bowring S., Iizuka T., Komiya T., Lepland A., Rosing M. T. and Ueno Y. (2013) The oxygen isotope composition of earth's oldest rocks and evidence of a terrestrial magma ocean. *Geochem. Geophys. Geosyst.* **14**. http://dx.doi.org/10.1002/ggge.20128.

Schröder S., Lacassie J. P. and Beukes N. J. (2006) Stratigraphic and geochemical framework of the Agouron drill cores, Transvaal Supergroup (Neoarchean-Paleoproterozoic, South Africa). *S. Afr. J. Geol.* **109**, 23–54.

Spicuzza M. J., Day J. M. D., Taylor L. A. and Valley J. W. (2007) Oxygen isotope constraints on the origin and differentiation of the Moon. *Earth Planet. Sci. Lett.* **253**, 254–265.

Tanaka R. and Nakamura E. (2013) Determination of ^{17}O-excess of terrestrial silicate/oxide minerals with respect to Vienna Standard Mean Ocean Water (VSMOW). *Rapid Commun. Mass Spectrom.* **27**, 285–297.

Thiemens M. H., Jackson T., Zipf E. C., Erdman P. W. and van Egmond C. (1995) Carbon dioxide and oxygen isotope anomalies in the mesosphere and stratosphere. *Science* **270**, 969–972.

Tsikos H., Beukes N. J., Moore J. M. and Harris C. (2003) Deposition, diagenesis, and secondary enrichment of metals in the Paleoproterozoic Hotazel Iron Formation, Kalahari Manganese Field, South Africa. *Econ. Geol.* **98**, 1449–1462.

Uemura R., Barkan E., Abe O. and Luz B. (2010) LLTriple isotope composition of oxygen in atmospheric water vapor. *Geophys. Res. Lett.* **37**.

Valley J. W., Kitchen N., Kohn M. J., Niendorf C. R. and Spicuzza M. J. (1995) UWG-2, a garnet standard for oxygen isotope ratios: strategies for high precision and accuracy with laser heating. *Geochim. Cosmochim. Acta* **59**, 5223–5231.

Wiechert U. H., Halliday A. N., Palme H. and Rumble D. (2004) Oxygen isotope evidence for rapid mixing of the HED meteorite parent body. *Earth Planet. Sci. Lett.* **221**, 373–382.

Whitehouse M. J., Kamber B. S. and Moorbath S. (1999) Age significance of U–Th–Pb zircon data from early Archaean rocks of west Greenland—a reassessment based on combined ion-microprobe and imaging studies. *Chem. Geol.* **160**, 201–224.

Whitehouse M. J., Myers J. S. and Fedo C. M. (2009) The Akilia Controversy: field, structural and geochronological evidence questions interpretations of >3.8 Ga life in SW Greenland. *J. Geol. Soc. London* **166**, 335–348.

York D. (1969) Least squares fitting of a straight line with correlated errors. *Earth Planet. Sci. Lett.* **5**, 320–324.

Young E. D., Galy A. and Nagahara H. (2002) Kinetic and equilibrium mass-dependent isotope fractionation laws in nature and their geochemical and cosmochemical significance. *Geochim. Cosmochim. Acta* **66**, 1095–1104.

Zheng Y.-F. (1991) Calculation of oxygen isotope fractionation in metal oxides. *Geochim. Cosmochim. Acta* **55**, 2299–2307.

Associate editor: Qing-Zhu Yin